Laboratory activity 3: Position control of a DC servomotor with resonant load
(Theoretical background)

Riccardo Antonello*   Francesco Ticozzi*

April 14, 2025

1   Activity goal

The goal of this laboratory activity is to design a position controller for a DC servomotor driving a *resonant* mechanical load. For such purpose, the original *inertial* load (disc inertia) of the DC gearmotor available in laboratory is replaced with a rigid beam connected to the motor through a flexible coupling (elastic joint). The whole setup actually resembles a conventional two–mass system, which is the representative model of practically every motion system with an elastic transmission. Both the PID and state–space control techniques are taken into account for the design. The state–space design is performed with either conventional eigenvalues placement methods, or by using optimal techniques based on the Linear Quadratic Regulator (LQR).

2   Activity goal

3   Analytical model of the DC gearmotor with resonant load

3.1   Equations of motion

The lumped–element diagram of the Quanser SRV–02 gearmotor with resonant load is shown in Fig. 1. The resonant load consists of two masses (*hub* and *beam* inertias) connected together by
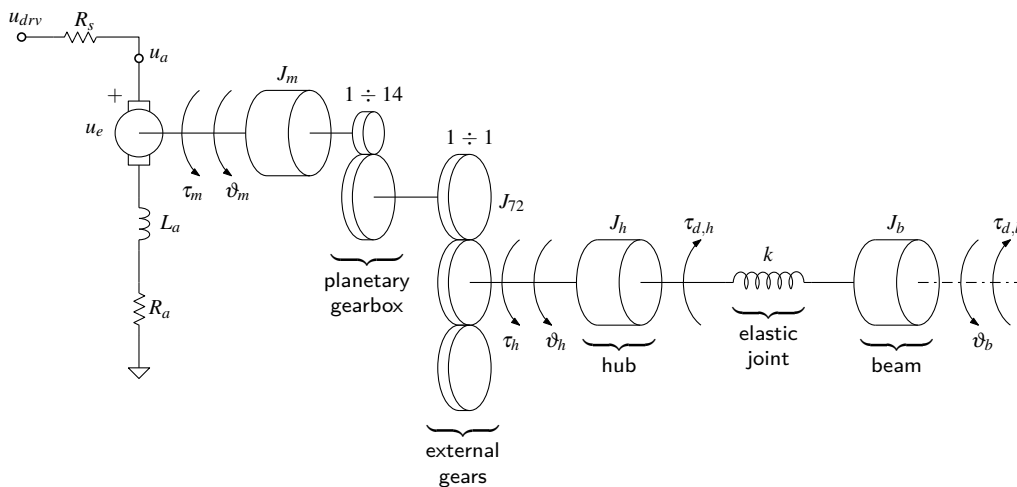

Figure 1: DC gearmotor with elastic joint: lumped–element diagram.

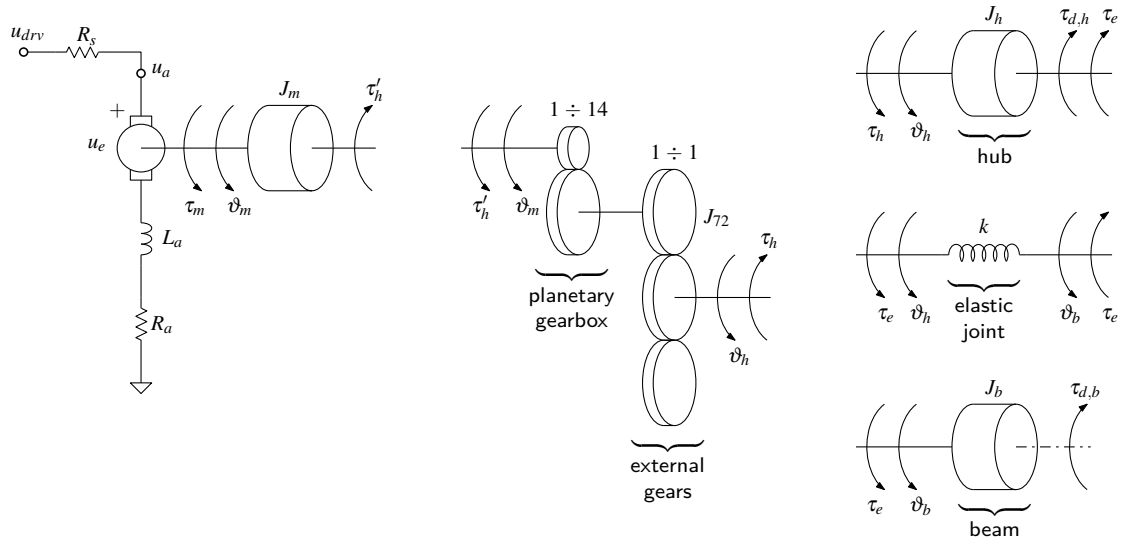*Dept. of Information Engineering (DEI), University of Padova; email: {antonello, ticozzi}@dei.unipd.it

Figure 2: DC gearmotor with elastic joint: free–body diagram.

J_b, B_b	beam moment of inertia and viscous friction coefficient
J_h, B_h	hub moment of inertia and viscous friction coefficient
k	elastic joint spring (stiffness) constant
τ_h, ω_h, ϑ_h	hub torque, speed and position
ω_b, ϑ_b	beam speed and position
ϑ_d	beam displacement angle, i.e. $\vartheta_d \triangleq \vartheta_b - \vartheta_h$
$\tau_{d,h}$	disturbance torque applied on hub inertia
$\tau_{d,b}$	disturbance torque applied on beam inertia

Table 1: DC gearmotor with elastic joint: additional symbols definitions.

means of an elastic joint. The voltage amplifier driving the DC gearmotor is omitted in Fig. 1 for space limitation reasons. For a detailed description of the DC gearmotor and the voltage driver, and their related dynamical models, refer to the handout of laboratory activity 0. In addition to the original notation introduced there, the additional symbols of Tab. 1 are introduced for the resonant load case. In order to simplify the notation, it will be assumed that the hub inertia J_h also accounts for the inertia of the three external gears, namely $J_h = J'_h + 3\,J_{72}$, with J'_h being the actual hub inertia.

With the aid of the free–body diagram reported in Fig. 2 (which highlights, for each body, all the external and internal torques exerted *on* the body by the environment and the other bodies), the following lumped–parameter LTI model of the DC gearmotor with elastic joint can be derived:

$$\begin{cases} L_a \dfrac{di_a}{dt} + (R_a + R_s)\, i_a \;=\; u_{drv} - u_e & \text{(electrical dynamics)} \quad (1) \\[2.2ex] J_m \dfrac{d\omega_m}{dt} + B_m\, \omega_m \;=\; \tau_m - \tau_h' & \text{(rotor mechanical dynamics)} \quad (2) \\[2.2ex] J_h \dfrac{d\omega_h}{dt} + B_h\, \omega_h \;=\; \tau_h - \tau_e - \tau_{d,h} & \text{(hub mechanical dynamics)} \quad (3) \\[2.2ex] J_b \dfrac{d\omega_b}{dt} + B_b\, \omega_b \;=\; \tau_e - \tau_{d,b} & \text{(beam mechanical dynamics)} \quad (4) \end{cases}$$

together with the motor equations

$$\begin{cases} u_e \;=\; k_e\, \omega_m & \text{(law of generators)} \quad (5) \\[1.8ex] \tau_m \;=\; k_t\, i_a & \text{(law of motors)} \quad (6) \end{cases}$$

plus the gearbox conditions

$$\begin{cases} \omega_h \;=\; \omega_m/N & \text{(gearbox speed transformation)} \quad (7) \\[1.8ex] \tau_h \;=\; N\, \tau_h' & \text{(gearbox torque transformation)} \quad (8) \end{cases}$$

and the elastic joint torque

$$\tau_e \;=\; k\,(\vartheta_h - \vartheta_b) \qquad \text{(elastic joint torque)} \quad (9)$$

The equation (8) is derived from the power balance of an ideal gearbox with a 100% efficiency, i.e. by assuming that the gearbox mechanical input power $P_m = \tau_h'\, \omega_m$ is equal to the output power $P_h = \tau_h\, \omega_h$. The torque $\tau_{d,h}$ in (3) represents a generic disturbance torque exerted on the hub body. In this handout, it is used to account for the *Coulomb* (*static*) friction of the mechanical transmission. The Coulomb friction consists of a constant resistant torque which opposes to the load movement, namely

$$\tau_{d,h} \;=\; \tau_{sf}\, \mathrm{sign}(\omega_l)\,, \qquad \tau_{sf} > 0 \qquad \text{(Coulomb friction at \textit{hub side})} \quad (10)$$

The torque $\tau_{d,b}$ in (4) represents a generic disturbance torque applied to the beam. In this handout, it is assumed equal to zero, under the assumption that no external torques are applied to the beam. The voltage u_{drv} in (1) is provided by the voltage driver with dynamics

$$T_{drv} \dfrac{du_{drv}}{dt} + u_{drv} \;=\; k_{drv}\, u \qquad \text{(voltage driver dynamics)} \quad (11)$$

where k_{drv} and T_{drv} are the driver DC gain and dominant time constant.

The rotor+hub mechanical dynamics can be obtained by combining (2)–(3) with (5)–(8); at *motor side*, it holds that

$$J_{eq} \dfrac{d\omega_m}{dt} + B_{eq}\, \omega_m \;=\; \tau_m - \dfrac{1}{N}\, \tau_{d,h} - \dfrac{1}{N}\, \tau_e \qquad \left(\begin{array}{c} \text{rotor+hub mechanical dynamics} \\ \text{at \textit{motor side}} \end{array} \right) \quad (12)$$

where

$$J_{eq} \;=\; J_m + \frac{J_h}{N^2}\,, \qquad B_{eq} \;=\; B_m + \frac{B_h}{N^2} \tag{13}$$

are the total inertia and viscous friction "seen" at *motor side*. Alternatively, at *hub side*, the rotor+hub mechanical dynamics becomes

$$N^2 J_{eq} \frac{d\omega_h}{dt} + N^2 B_{eq}\,\omega_h \;=\; N\,\tau_m - \tau_{d,h} - \tau_e \qquad \left(\begin{array}{c} \text{rotor+hub mechanical dynamics} \\ \text{at } \textit{hub side} \end{array} \right) \tag{14}$$

with $N^2 J_{eq}$ and $N^2 B_{eq}$ being the total inertia and viscous friction "seen" at *hub side*. From (12), note that the total friction torque generated at motor side is equal to

$$\tau_f' \;=\; B_{eq}\,\omega_m + \frac{\tau_{sf}}{N}\operatorname{sign}(\omega_m) \qquad \text{(total friction at } \textit{motor side}\text{)} \tag{15}$$

which consists of the sum of the viscous and Coulomb friction terms. At hub side, the total friction is equal to

$$\tau_f \;=\; N\,\tau_f' \;=\; N^2 B_{eq}\,\omega_l + \tau_{sf}\operatorname{sign}(\omega_l) \qquad \text{(total friction at } \textit{hub side}\text{)} \tag{16}$$

The overall mechanical dynamics is described by the two equations (12) and (4), that are coupled via the elastic torque (9). It holds that

$$\begin{cases} J_{eq} \dfrac{d^2\vartheta_m}{dt^2} + B_{eq} \dfrac{d\vartheta_m}{dt} + \dfrac{k}{N^2}\vartheta_m - \dfrac{k}{N}\vartheta_b \;=\; \tau_m - \dfrac{1}{N}\tau_{d,h} \\[2mm] J_b \dfrac{d^2\vartheta_b}{dt^2} + B_b \dfrac{d\vartheta_b}{dt} + k\,\vartheta_b - \dfrac{k}{N}\vartheta_m \;=\; 0 \end{cases} \qquad \left(\begin{array}{c} \text{overall mechanical} \\ \text{dynamics} \end{array} \right) \tag{17}$$

where in the second equation it has been used the assumption $\tau_{d,b} = 0$. By using (7)–(8), it can be alternatively written for the two load side variables ϑ_h and ϑ_b, i.e.

$$\begin{cases} N^2 J_{eq} \dfrac{d^2\vartheta_h}{dt^2} + N^2 B_{eq} \dfrac{d\vartheta_h}{dt} + k\,\vartheta_h - k\,\vartheta_b \;=\; N\,\tau_m - \tau_{d,h} \\[2mm] J_b \dfrac{d^2\vartheta_b}{dt^2} + B_b \dfrac{d\vartheta_b}{dt} + k\,\vartheta_b - k\,\vartheta_h \;=\; 0 \end{cases} \tag{18}$$

The overall system dynamics is given by the combination of (1), (11) and (17):

$$\begin{cases} L_a \dfrac{di_a}{dt} + R_{eq}\,i_a \;=\; u_{drv} - k_e \dfrac{d\vartheta_m}{dt} \\[2mm] T_{drv} \dfrac{du_{drv}}{dt} + u_{drv} \;=\; k_{drv}\,u \\[2mm] J_{eq} \dfrac{d^2\vartheta_m}{dt^2} + B_{eq} \dfrac{d\vartheta_m}{dt} + \dfrac{k}{N^2}\vartheta_m - \dfrac{k}{N}\vartheta_b \;=\; k_t\,i_a - \dfrac{1}{N}\tau_{d,h} \\[2mm] J_b \dfrac{d^2\vartheta_b}{dt^2} + B_b \dfrac{d\vartheta_b}{dt} + k\,\vartheta_b - \dfrac{k}{N}\vartheta_m \;=\; 0 \end{cases} \qquad \left(\begin{array}{c} \text{overall system} \\ \text{dynamics} \end{array} \right) \tag{19}$$

where in the first equation it has been used the law of generators (5), and the definition

$$R_{eq} \;=\; R_a + R_s \,, \tag{20}$$

Hub moment of inertia	J_h	$6.84 \times 10^{-4}\,\mathrm{kgm^2}$ [1]
Hub viscous friction coefficient	B_h	estimated in previous lab activity [2]
Hub side Coulomb friction	τ_{sf}	estimated in previous lab activity
Beam moment of inertia	J_b	$1.4 \times 10^{-3}\,\mathrm{kgm^2}$ [1]
Beam viscous friction coefficient	B_b	to be estimated
Joint stiffness	k	to be estimated

[1] The parameters refer to the "aluminum hub". For the "Quanser hub", the parameters are:

- hub moment of inertia: $J_h = 5.1 \times 10^{-4}\,\mathrm{kgm^2}$
- beam moment of inertia: $J_b = 2.0 \times 10^{-3}\,\mathrm{kgm^2}$

[2] It is assumed equal to the coefficient B_l of the inertial load case. Therefore, the coefficient B_{eq} in (13) is equivalent to the quantity $B_{eq} = B_m + B_l/N^2$ estimated in the laboratory activity 0.

Table 2: Resonant load parameters.

while in the third equation it has been used the law of motors (6). The model can be alternatively rewritten in terms of load side variables, simply by replacing the last two equations in (19) with (18). The nominal parameters of the resonant mechanical load are summarised in Tab. 2.

3.2 Transfer functions

After applying the $\mathcal{L}$–transform to both sides of each equation in (19), the block diagram of Fig. 3a can be easily derived. In control applications that involve mechanical systems with structural flexibility, it is customary to introduce the following definitions:

- *collocated system*: there is no flexibility between the sensor and the actuator, i.e. the two are placed on the same rigid body.

- *non–collocated system*: there is a flexibility between the sensor and the actuator, i.e. the two are placed on different bodies, which are connected each other through an elastic coupling.

Assuming the motor torque τ_m as the actuation variable, and the hub and beam positions ϑ_h and ϑ_b as the measured variables, it is immediate to derive from (18) the following expressions for the transfer functions of the collocated and non–collocated systems:

$$P_{\tau_m \to \vartheta_h}(s) \;=\; \frac{\theta_h(s)}{\tau_m(s)} \;=\; \frac{1}{N} \cdot \frac{J_b\,s^2 \,+\, B_b\,s \,+\, k}{D_\tau(s)} \qquad \text{(collocated system tf)} \qquad (21)$$

$$P_{\tau_m \to \vartheta_b}(s) \;=\; \frac{\theta_b(s)}{\tau_m(s)} \;=\; \frac{1}{N} \cdot \frac{k}{D_\tau(s)} \qquad \text{(non–collocated system tf)} \qquad (22)$$

with

$$D_\tau(s) \;=\; \left(J_{eq}\,s^2 \,+\, B_{eq}\,s \,+\, \frac{k}{N^2} \right)\left(J_b\,s^2 \,+\, B_b\,s \,+\, k \right) \,-\, \left(\frac{k}{N} \right)^2 \qquad (23)$$

$$= \; s^2\,(J_{eq}s \,+\, B_{eq})\,(J_b s \,+\, B_b) \,+\, k\,s\left[\left(J_{eq} \,+\, \frac{J_b}{N^2} \right) s \,+\, \left(B_{eq} \,+\, \frac{B_b}{N^2} \right) \right] \qquad (24)$$

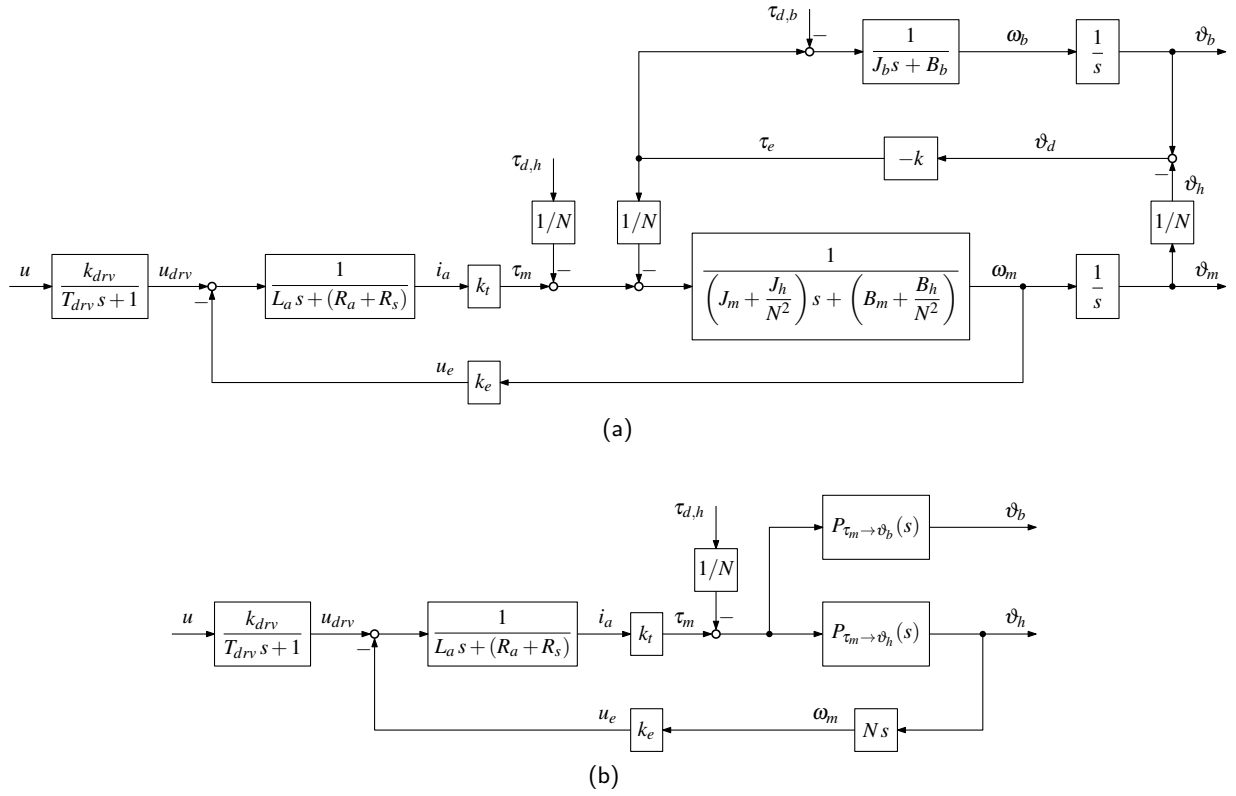$$= \; s\,D_\tau'(s) \qquad (25)$$

Figure 3: DC gearmotor with elastic joint: block diagram.

and

$$D'_\tau(s) = J_{eq} J_b s^3 + (J_{eq} B_b + J_b B_{eq}) s^2 + \left[B_{eq} B_b + k \left(J_{eq} + \frac{J_b}{N^2} \right) \right] s + k \left(B_{eq} + \frac{B_b}{N^2} \right) \tag{26}$$

With (21) and (22), the block diagram of Fig. 3a can be reduced to that of Fig. 3b; then, by assuming the driver input voltage u as the new actuation variable, the transfer functions of the collocated and non–collocated systems become:

$$P_{u \to \vartheta_h}(s) = \frac{\vartheta_h(s)}{u(s)} = \frac{k_{drv}}{T_{drv}s + 1} \cdot \frac{\dfrac{k_t}{L_a s + R_{eq}} P_{\tau_m \to \vartheta_h}(s)}{1 + \dfrac{k_t k_e N s}{L_a s + R_{eq}} P_{\tau_m \to \vartheta_h}(s)} \tag{27}$$

$$= \frac{k_{drv}}{T_{drv}s + 1} \cdot \frac{1}{N s} \cdot \frac{k_t \left(J_b s^2 + B_b s + k \right)}{(L_a s + R_{eq}) D'_\tau(s) + k_t k_e \left(J_b s^2 + B_b s + k \right)} \tag{28}$$

$$P_{u \to \vartheta_b}(s) = \frac{\vartheta_b(s)}{u(s)} = \frac{k_{drv}}{T_{drv}s + 1} \cdot \frac{\dfrac{k_t}{L_a s + R_{eq}} P_{\tau_m \to \vartheta_b}(s)}{1 + \dfrac{k_t k_e N s}{L_a s + R_{eq}} P_{\tau_m \to \vartheta_h}(s)} \tag{29}$$

$$= \frac{k_{drv}}{T_{drv}s + 1} \cdot \frac{1}{N s} \cdot \frac{k_t \, k}{(L_a s + R_{eq}) D'_\tau(s) + k_t k_e \left(J_b s^2 + B_b s + k \right)} \tag{30}$$

Since the measurement provided by the potentiometer installed on the hub ("potentiometer 2") measures the beam displacement angle $\vartheta_d = \vartheta_b - \vartheta_h$, it makes sense to derive the system transfer functions also for such output. By subtracting (21) from (22), and (28) from (30), it follows that:

$$P_{\tau_m \to \vartheta_d}(s) = \frac{\vartheta_d(s)}{\tau_m(s)} = -\frac{1}{N} \cdot \frac{J_b\, s + B_b}{D'_\tau(s)} \tag{31}$$

$$P_{u \to \vartheta_d}(s) = \frac{\vartheta_d(s)}{U(s)} = -\frac{k_{drv}}{T_{drv}s + 1} \cdot \frac{1}{N} \cdot \frac{k_t\,(J_b\, s + B_b)}{(L_a\, s + R_{eq})\, D'_\tau(s) + k_t\, k_e\,(J_b\, s^2 + B_b\, s + k)} \tag{32}$$

Typically, the time constants of the voltage driver and the armature circuit are both very small, i.e.

$$L_a/R_{eq} \ll 1\,, \qquad T_{drv} \ll 1 \tag{33}$$

so that the transfer functions (28), (30) and (32) can be simplified as follows

$$P_{u \to \vartheta_h}(s) = \frac{\vartheta_h(s)}{u(s)} = \frac{1}{Ns} \cdot \frac{k_{drv}\, k_t\,(J_b\, s^2 + B_b\, s + k)}{R_{eq}\, D'_\tau(s) + k_t\, k_e\,(J_b\, s^2 + B_b\, s + k)} \tag{34}$$

$$P_{u \to \vartheta_b}(s) = \frac{\vartheta_b(s)}{u(s)} = \frac{1}{Ns} \cdot \frac{k_{drv}\, k_t\, k}{R_{eq}\, D'_\tau(s) + k_t\, k_e\,(J_b\, s^2 + B_b\, s + k)} \tag{35}$$

$$P_{u \to \vartheta_d}(s) = \frac{\vartheta_d(s)}{u(s)} = -\frac{1}{N} \cdot \frac{k_{drv}\, k_t\,(J_b\, s + B_b)}{R_{eq}\, D'_\tau(s) + k_t\, k_e\,(J_b\, s^2 + B_b\, s + k)} \tag{36}$$

Notes:

1) Reconsider the two transfer functions (21) and (22), and assume that the system has no damping, i.e. $B_{eq} = B_b = 0$. Then

$$P_{\tau_m \to \vartheta_h}(s) = \frac{1}{N} \cdot \frac{1}{J_{eq}s^2} \cdot \frac{s^2 + \dfrac{k}{J_b}}{s^2 + \left(\dfrac{k}{J_b} + \dfrac{k}{J_{eq}\, N^2}\right)} \tag{37}$$

$$P_{\tau_m \to \vartheta_b}(s) = \frac{1}{N} \cdot \frac{1}{J_{eq}s^2} \cdot \frac{\dfrac{k}{J_b}}{s^2 + \left(\dfrac{k}{J_b} + \dfrac{k}{J_{eq}\, N^2}\right)} \tag{38}$$

The two transfer functions have the same denominator, and differ only in their numerators: in particular, the collocated system has a pair of complex conjugate zeros, while the non–collocated system has no zeros. The frequencies of the complex conjugate zeros and poles are

$$\omega_z = \sqrt{\frac{k}{J_b}}\,, \qquad \omega_p = \sqrt{\frac{k}{J_b} + \frac{k}{J_{eq}\, N^2}} \tag{39}$$

A pair of complex conjugate poles produces a peak in the frequency response magnitude, called

resonance; vice versa, a pair of complex conjugate zeros produces a dip in the the frequency response magnitude, called *antiresonance*. From (39), it can be noticed that the antiresonance has a smaller frequency than the resonance, i.e. $0 < \omega_z < \omega_p$. This condition is always true in a mechanical system with flexibilities: in particular, for systems with multiple modes (i.e. whose lumped element diagram resembles a multi spring–mass system), it can be shown that the collocated system always has the poles and zeros alternating along the imaginary axis, with a zero located between two consecutive poles (zeros "sandwiched" between consecutive poles).

The double integrator in (37) and (38) represents the "rigid body mode". When $k \to 0$ it holds that

$$P_{\tau_m \to \vartheta_h}(s) \quad \xrightarrow{k \to 0} \quad \frac{1}{N} \cdot \frac{1}{J_{eq} s^2} \tag{40}$$

$$P_{\tau_m \to \vartheta_b}(s) \quad \xrightarrow{k \to 0} \quad 0 \tag{41}$$

which is consistent with the fact that in case of an "infinitely soft" spring, no interaction exists between the hub and beam inertias, and the system behaves as a single inertia system, with inertia equal to J_{eq} (which is the only inertia rigidly connected to the actuator).

When $k \to +\infty$ it holds that

$$P_{\tau_m \to \vartheta_h}(s) \quad \xrightarrow{k \to +\infty} \quad \frac{1}{N} \cdot \frac{1}{\left(J_{eq} + \dfrac{J_b}{N^2} \right) s^2} \tag{42}$$

$$P_{\tau_m \to \vartheta_b}(s) \quad \xrightarrow{k \to +\infty} \quad \frac{1}{N} \cdot \frac{1}{\left(J_{eq} + \dfrac{J_b}{N^2} \right) s^2} \tag{43}$$

which is consistent with the fact that in case of an "infinitely rigid" spring, the system behaves again as a single inertia system, with inertia equal to the sum of the inertias (as "seen" at motor side) J_{eq} and J_b/N^2.

2) The transfer function from the hub position ϑ_h to the beam position ϑ_b can be determined by computing the ratio between (22) and (21), i.e.

$$
\begin{aligned}
P_{\vartheta_h \to \vartheta_b}(s) &= \frac{\vartheta_b(s)}{\vartheta_h(s)} = \frac{P_{\vartheta_b \to \tau_m}(s)}{P_{\vartheta_h \to \tau_m}(s)} = \frac{k}{J_b s^2 + B_b s + k} \\
\cdots &= \frac{\omega_z^2}{s^2 + 2\delta_z \omega_z s + \omega_z^2} \quad \text{with} \quad \delta_z = \frac{B_b}{2\sqrt{J_b k}}
\end{aligned}
\tag{44}
$$

The transfer function (44) reveals the "meaning" of the antiresonance frequency ω_z: it is the frequency at which the inertia J_b oscillates when it is perturbed from its equilibrium state, while the hub position is maintained locked. Conversely, the resonance frequency ω_p is the frequency at which the two–inertia system oscillates when it is perturbed from its equilibrium state, and no external forcing is applied. The previous interpretation for the antiresonance frequency will be used in Sec. 5 to estimate the elastic joint stiffness k and the beam viscous friction coefficient B_h.

3.3 State space model

With the simplifying assumptions (33), the first two differential equations in (19) can be reduced to the following two algebraic equations:

$$\frac{L_a}{R_{eq}} \frac{di_a}{dt} + i_a = \frac{1}{R_{eq}} \left(u_{drv} - k_e \frac{d\vartheta_m}{dt} \right) \xrightarrow{\ L_a/R_{eq} \to 0\ } i_a = \frac{1}{R_{eq}} \left(u_{drv} - k_e \frac{d\vartheta_m}{dt} \right) \quad (45)$$

$$T_{drv} \frac{du_{drv}}{dt} + u_{drv} = k_{drv}\, u \xrightarrow{\ T_{drv} \to 0\ } u_{drv} = k_{drv}\, u \quad (46)$$

With these two algebraic conditions, the overall system dynamics (19), rewritten for the two load side variables ϑ_h and ϑ_b, simplifies as follows[1]:

$$\begin{cases} N^2 J_{eq}\, \ddot{\vartheta}_h + N^2 \left(B_{eq} + \dfrac{k_t\, k_e}{R_{eq}} \right) \dot{\vartheta}_h + k\,\vartheta_h - k\,\vartheta_b = \dfrac{N\, k_t\, k_{drv}}{R_{eq}}\, u - \tau_{d,h} \\[2ex] J_b\, \ddot{\vartheta}_b + B_b\, \dot{\vartheta}_b + k\,\vartheta_b - k\,\vartheta_h = 0 \end{cases} \quad (47)$$

Define the state vector $\boldsymbol{x} = [\vartheta_h,\ \vartheta_b,\ \dot{\vartheta}_h,\ \dot{\vartheta}_b]^T$: then, after solving (47) for the accelerations variables $\ddot{\vartheta}_h$ and $\ddot{\vartheta}_b$, it is immediate to derive the following state–space model:

$$\dot{\boldsymbol{x}} = \boldsymbol{A}\,\boldsymbol{x} + \boldsymbol{B}\,u + \boldsymbol{B}_d\,\tau_{d,h} \quad (48)$$

with

$$\boldsymbol{A} = \begin{bmatrix} 0 & 0 & 1 & 0 \\[1ex] 0 & 0 & 0 & 1 \\[1ex] -\dfrac{k}{N^2 J_{eq}} & \dfrac{k}{N^2 J_{eq}} & -\dfrac{1}{J_{eq}} \left(B_{eq} + \dfrac{k_t\, k_e}{R_{eq}} \right) & 0 \\[2ex] \dfrac{k}{J_b} & -\dfrac{k}{J_b} & 0 & -\dfrac{B_b}{J_b} \end{bmatrix} \quad (49)$$

$$\boldsymbol{B} = \begin{bmatrix} 0 \\[1ex] 0 \\[1ex] \dfrac{k_t\, k_{drv}}{N\, J_{eq}\, R_{eq}} \\[2ex] 0 \end{bmatrix}, \qquad \boldsymbol{B}_d = \begin{bmatrix} 0 \\[1ex] 0 \\[1ex] -\dfrac{1}{N^2 J_{eq}} \\[2ex] 0 \end{bmatrix} \quad (50)$$

An alternative state–space model can be obtained by redefining the state vector in terms of the two measured variables ϑ_h and $\vartheta_d = \vartheta_b - \vartheta_h$, namely $\boldsymbol{x}' = [\vartheta_h,\ \vartheta_d,\ \dot{\vartheta}_h,\ \dot{\vartheta}_d]^T$. The new state $\boldsymbol{x}'$ is related to the previous state $\boldsymbol{x}$ by the state transformation

$$\boldsymbol{x} = \boldsymbol{T}\,\boldsymbol{x}' \qquad \text{with} \qquad \boldsymbol{T} = \begin{bmatrix} 1 & 0 & 0 & 0 \\ 1 & 1 & 0 & 0 \\ 0 & 0 & 1 & 0 \\ 0 & 0 & 1 & 1 \end{bmatrix} \quad (51)$$

---

[1]The "dot" notation $\dot{x} = dx/dt$ and $\ddot{x} = d^2x/dt^2$ is used in the following to ease the writing of the equations.

The state–space model in the new state vector is

$$\dot{\boldsymbol{x}}' \;=\; \boldsymbol{A}'\,\boldsymbol{x}' \;+\; \boldsymbol{B}'\,u \;+\; \boldsymbol{B}'_d\,\tau_{d,h} \tag{52}$$

with

$$\boldsymbol{A}' \;=\; \boldsymbol{T}^{-1}\,\boldsymbol{A}\,\boldsymbol{T} \;=\; \begin{bmatrix} 0 & 0 & 1 & 0 \\[2mm] 0 & 0 & 0 & 1 \\[2mm] 0 & \dfrac{k}{N^2\,J_{eq}} & -\dfrac{1}{J_{eq}}\left(B_{eq} + \dfrac{k_t\,k_e}{R_{eq}}\right) & 0 \\[4mm] 0 & -\dfrac{k}{J_b} - \dfrac{k}{J_{eq}\,N^2} & -\dfrac{B_b}{J_b} + \dfrac{1}{J_{eq}}\left(B_{eq} + \dfrac{k_t\,k_e}{R_{eq}}\right) & -\dfrac{B_b}{J_b} \end{bmatrix} \tag{53}$$

$$\boldsymbol{B}' \;=\; \boldsymbol{T}^{-1}\boldsymbol{B} \;=\; \begin{bmatrix} 0 \\[2mm] 0 \\[2mm] \dfrac{k_t\,k_{drv}}{N\,J_{eq}\,R_{eq}} \\[4mm] -\dfrac{k_t\,k_{drv}}{N\,J_{eq}\,R_{eq}} \end{bmatrix}, \qquad \boldsymbol{B}'_d \;=\; \boldsymbol{T}^{-1}\boldsymbol{B_d} \;=\; \begin{bmatrix} 0 \\[2mm] 0 \\[2mm] -\dfrac{1}{N^2 J_{eq}} \\[4mm] \dfrac{1}{N^2 J_{eq}} \end{bmatrix} \tag{54}$$

4 Analytical model of the resonant load

The resonant load available in laboratory is shown in Fig. 4a. In the picture, ① is a rigid beam, ② a pre–stretched linear spring and ③ the hub unit that can be connected to the output shaft of the Quanser SRV–02 servomotor. The hub unit contains a potentiometer (potentiometer "2") that measures the beam deflection ϑ_d with respect to its rest position (see Fig. 4b and 4c). The relationship existing between the elastic restoring torque τ_e and the beam angular displacement ϑ_d is in general nonlinear, but it can be linearised for small displacements to yield the expression of a conventional torsional spring with linear characteristic, lumped on the beam pivot. To determine the general expression of the restoring torque, start by considering the restoring forces that are generated by the two linear springs when the beam is deflected from its rest position. With reference to Fig. 4b–4c, it holds that

$$F_1 \;=\; k_s\,(L_1 - L) + F_r\,, \qquad F_2 \;=\; k_s\,(L_2 - L) + F_r \tag{55}$$

where F_r is the initial tension of the two linear springs due to the pre–stretching. The length of the two springs when the beam is at rest position is equal to

$$L \;=\; \sqrt{r^2 + (R - d)^2} \tag{56}$$

When the beam is deflected from its rest position, the lengths of the two springs become

$$L_1 \;=\; \sqrt{L_{1,x}^2 + L_{1,y}^2}\,, \qquad L_2 \;=\; \sqrt{L_{2,x}^2 + L_{2,y}^2} \tag{57}$$

where

$$L_{1,x} = r + R\sin\vartheta_d \,, \qquad L_{2,x} = r - R\sin\vartheta_d \,, \qquad L_{1,y} = L_{2,y} = R\cos\vartheta_d - d \qquad (58)$$

The horizontal and vertical components of the two restoring forces can be easily obtained from triangle similarity considerations. It can be verified that

$$F_{1,x} = F_1\frac{L_{1,x}}{L_1} \,, \qquad F_{1,y} = F_1\frac{L_{1,y}}{L_1} \,, \qquad F_{2,x} = F_2\frac{L_{2,x}}{L_2} \,, \qquad F_{2,y} = F_2\frac{L_{2,y}}{L_2} \qquad (59)$$

These force components can be used to compute the restoring torque. With the sign conventions of Fig. 4c, it holds that

$$\tau_e = (F_{2,x} - F_{1,x})\,R\cos\vartheta_d + (F_{1,y} + F_{2,y})\,R\sin\vartheta_d \qquad (60)$$

which shows that the restoring torque is a nonlinear function of the deflection angle. With a certain effort, it is possible to verify that the small angle linearisation is equal to

$$\tau_e = -k\,\vartheta_d \qquad \text{with} \qquad k = \left|\frac{\partial\tau_e(0)}{\partial\vartheta_d}\right| = \frac{2R}{L^3}\left[\left(d\,L^2 - R\,r^2\right)F_r + \left(r^2\,R\,L\right)k_s\right] \qquad (61)$$

which is the expression of the restoring torque of a conventional torsional spring (as the one considered in the previous Sec. 3 – see (9)) lumped on the beam pivot. Note that the equivalent stiffness k of the torsional spring depends both on the stiffness k_s and the initial tension F_r of the two springs. If these parameters were known, then the equivalent stiffness could be evaluated by resorting to the expression in (61). In practice, however, it is easier to estimate the equivalent stiffness by performing a simple experimental test, as described in the next section.
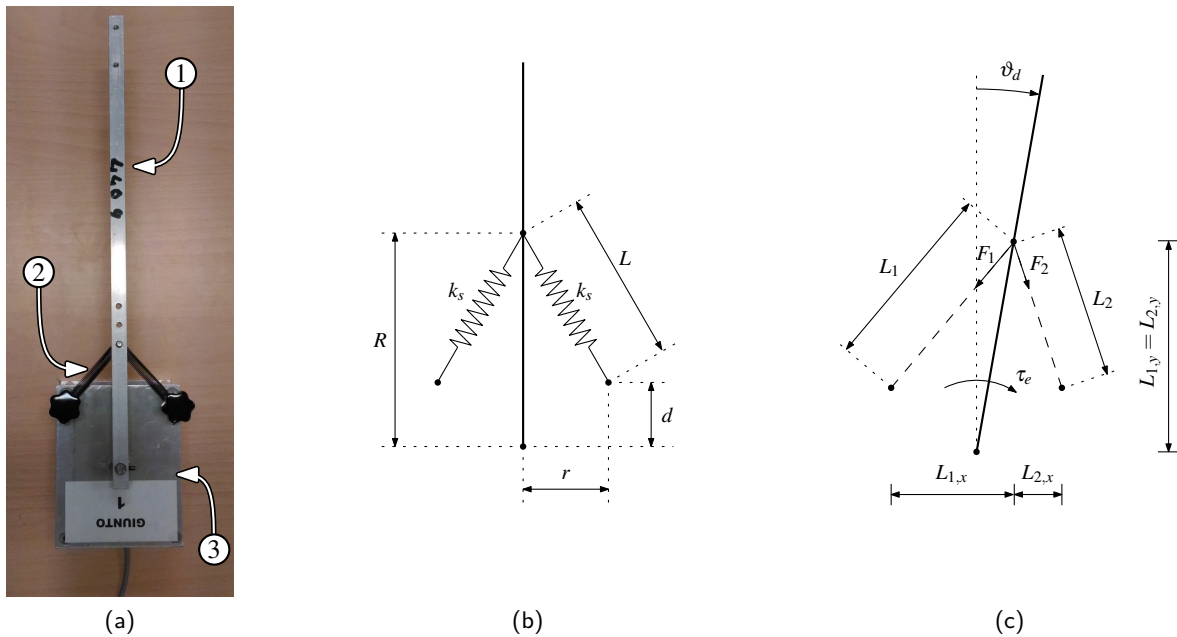

Figure 4: Flex joint: (a) photo (top view); (b) beam at rest position; (c) beam at deflected position.

5 Estimation of the elastic joint parameters

Reconsider the overall mechanical dynamics (17), and assume that the hub is kept fixed (i.e. $\omega_h = 0$). Moreover, assume that no external disturbance torque is applied to the beam (i.e. $\tau_{d,b} = 0$). Then, it can be verified that the beam displacement $\vartheta_d = \vartheta_b - \vartheta_h$ satisfies the homogeneous differential equation

$$J_b \ddot{\vartheta}_d + B_b \dot{\vartheta}_d + k \vartheta_d = 0 \tag{62}$$

which can be rewritten as follows

$$\ddot{\vartheta}_d + 2 \delta \omega_n \dot{\vartheta}_d + \omega_n^2 \vartheta_d = 0 \tag{63}$$

with

$$\omega_n = \sqrt{\frac{k}{J_b}}, \qquad \delta = \frac{B_b}{2\sqrt{J_b k}} \tag{64}$$

Typically $\delta < 1$, so that (63) represents an underdamped second order system with no external forcing. Its natural response to non–zero initial position and velocity conditions is

$$\vartheta_d(t) = A e^{\sigma t} \cos(\omega t + \phi) \tag{65}$$

where

$$\sigma = -\delta \omega_n, \qquad \omega = \omega_n \sqrt{1 - \delta^2} \tag{66}$$

and

$$A = \sqrt{\vartheta_d^2(0) + \left(\frac{\dot{\vartheta}_d(0) - \sigma \vartheta_d(0)}{\omega}\right)^2}, \qquad \phi = \text{atan}\left(\frac{\sigma \vartheta_d(0) - \dot{\vartheta}_d(0)}{\omega \vartheta_d(0)}\right) \tag{67}$$

The typical trend of the natural response (65) is shown in Fig. 5a. The damping and natural frequency of (63) can be estimated by measuring a certain number of local positive/negative peaks of (65), as explained in the following. For estimation purposes, consider the plot of the absolute value of (65), shown in Fig. 5b. The local peaks occur at the time instants

$$\omega t_k + \phi = k\pi \qquad \Rightarrow \qquad t_k = \frac{k\pi - \phi}{\omega}, \qquad k \in \mathbb{Z} \tag{68}$$
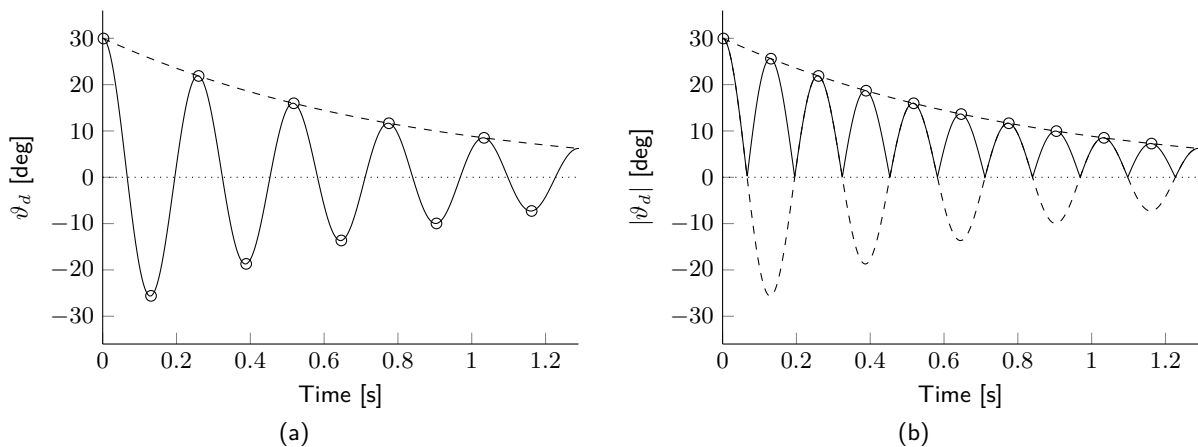

Figure 5: Typical natural response of an underdamped second order system: (a) natural response (with $\omega_n = 24.4\,\text{rad/s}$, $\delta = 0.05$ and $\vartheta_d(0) = 30°$, $\dot{\vartheta}(0) = 0$); (b) natural response – absolute value.

Their values are equal to

$$|\vartheta_d(t_k)| = A\, e^{\sigma\, t_k} \tag{69}$$

After k oscillations, the peak amplitude is reduced by a factor

$$\frac{|\vartheta_d(t_k)|}{|\vartheta_d(t_0)|} = e^{\sigma(t_k - t_0)} = \exp\left(-\frac{\delta\, k\, \pi}{\sqrt{1-\delta^2}}\right) \tag{70}$$

By taking the logarithm of both sides, expression (70) becomes

$$\log|\vartheta_d(t_k)| - \log|\vartheta_d(t_0)| = -k\,\xi \qquad \text{with} \qquad \xi = \frac{\delta\,\pi}{\sqrt{1-\delta^2}} \tag{71}$$

which is the equation of a straight line with slope ξ and intercept $\log|\vartheta_d(t_0)|$. Therefore, given the set of measurements

$$Z^M = \left\{t_k,\ |\vartheta_d(t_k)|\right\} \qquad \text{with} \quad k = 0,\, 1,\, \ldots,\, M-1 \tag{72}$$

which consists of M consecutive peaks of the absolute value of the natural response (65), the parameter ξ, also called *logarithmic decrement*, can be estimated by performing a linear least–square (LS) fitting (on the $(k, \log|\vartheta_d(t_k)|)$ plane) of the measured data. Let

$$z = -a\,k + b \tag{73}$$

be the straight line to fit on data. Introduce the notation

$$z = \boldsymbol{\varphi}_k^T\, \boldsymbol{\theta} \tag{74}$$

where

$$\boldsymbol{\varphi}_k^T = [-k,\ 1]\,, \qquad \boldsymbol{\theta} = [a,\ b]^T \tag{75}$$

are, respectively, the vectors of regressors and unknown parameters to be estimated. Then, the LS fitting can be determined by finding the value of $\boldsymbol{\theta}$ that minimises the quadratic error

$$V(\boldsymbol{\theta}) = \sum_{k=0}^{M-1} \left(\log|\vartheta(t_k)| - \boldsymbol{\varphi}_k^T\, \boldsymbol{\theta}\right)^2 \tag{76}$$

With the notation

$$\boldsymbol{Y} = \begin{bmatrix} \log|\vartheta(t_0)| \\ \log|\vartheta(t_1)| \\ \vdots \\ \log|\vartheta(t_{M-1})| \end{bmatrix} \in \mathbb{R}^{M\times 1}, \qquad \boldsymbol{\Phi} = \begin{bmatrix} \boldsymbol{\varphi}_0^T \\ \boldsymbol{\varphi}_1^T \\ \vdots \\ \boldsymbol{\varphi}_{M-1}^T \end{bmatrix} \in \mathbb{R}^{M\times 2} \tag{77}$$

the cost function can be rewritten as

$$V(\boldsymbol{\theta}) = [\boldsymbol{Y} - \boldsymbol{\Phi}\,\boldsymbol{\theta}]^T\, [\boldsymbol{Y} - \boldsymbol{\Phi}\,\boldsymbol{\theta}] \tag{78}$$

which is minimised by the least squares (LS) solution

$$\hat{\boldsymbol{\theta}}_{LS} \;=\; \left[\hat{a},\,\hat{b}\right]^{T} \;=\; \left(\boldsymbol{\Phi}^{T}\boldsymbol{\Phi}\right)^{-1}\boldsymbol{\Phi}^{T}\boldsymbol{Y} \tag{79}$$

Then, the LS estimate of the logarithmic decrement is $\hat{\xi} = \hat{a}$. Finally, by using the expression of the logarithmic decrement reported in (71), the following estimate of the damping factor can be retrieved

$$\hat{\delta} = \frac{\hat{\xi}}{\sqrt{\pi^2 + \hat{\xi}^2}} \tag{80}$$

For what regards the estimation of the natural frequency ω_n, let $T_k = t_{k+1} - t_k$ denote the measured time interval between two consecutive peaks. From (68) it follows that

$$\hat{\omega}_k \;=\; \pi/T_k \tag{81}$$

where $\hat{\omega}_k$ represents an estimate of the frequency ω obtained with the measurement T_k. Then, by averaging over all the possible measurements, the following estimate for the frequency ω results

$$\hat{\omega} \;=\; \frac{1}{M}\sum_{k=0}^{M-1}\hat{\omega}_k \tag{82}$$

Finally, by using (66) and (80), an estimate of the natural frequency ω_n is obtained as follows

$$\hat{\omega}_n \;=\; \frac{\hat{\omega}}{\sqrt{1 - \hat{\delta}^2}} \tag{83}$$

6 PID control design for collocated and non–collocated systems

6.1 Collocated control

The Bode plot of the collocated system (21) is shown in Fig. 6a. It is evident that a PD compensation of the type

$$C(s) \;=\; K_P + K_D\,s \;=\; K_P\,(1 + T_D\,s) \tag{84}$$

is sufficient to stabilize the closed–loop system for any choice of the gain crossover frequency ω_{gc} [2]. In Fig. 7 are shown the (positive) root loci with a P and PD compensations (for the PD compensation, the value $T_D = 1$ is used). The loci are parametrised with respect to the proportional gain K_P. From Fig. 7a, it is evident that the closed–loop system is stable for any choice of the proportional gain $K_P > 0$. The PD compensation (see Fig. 7b) introduces additional damping to the system, moving the root locus branches further inside the left–half complex plane.

6.2 Non–collocated control (optional)

The non–collocated system is more difficult to stabilize. In particular, a P or PD compensation destabilizes the closed–loop system if the proportional gain K_P is not small enough. This is evident from the two root loci reported in Fig. 8, obtained with the same P/PD compensators of the collocated case. There are basically two different methods for stabilising the non–collocated system:

▪ *Gain stabilization method* (or *gain–stabilized design*): the stability is achieved by forcing the magnitude of the frequency response to never exceed the unit value at high frequency. In particular, by forcing the resonant peak magnitude to be less than 1, it is guaranteed that no encirclements of the critical point occur in the Nyquist plot (of the loop transfer function), and hence the closed–loop system is stable.
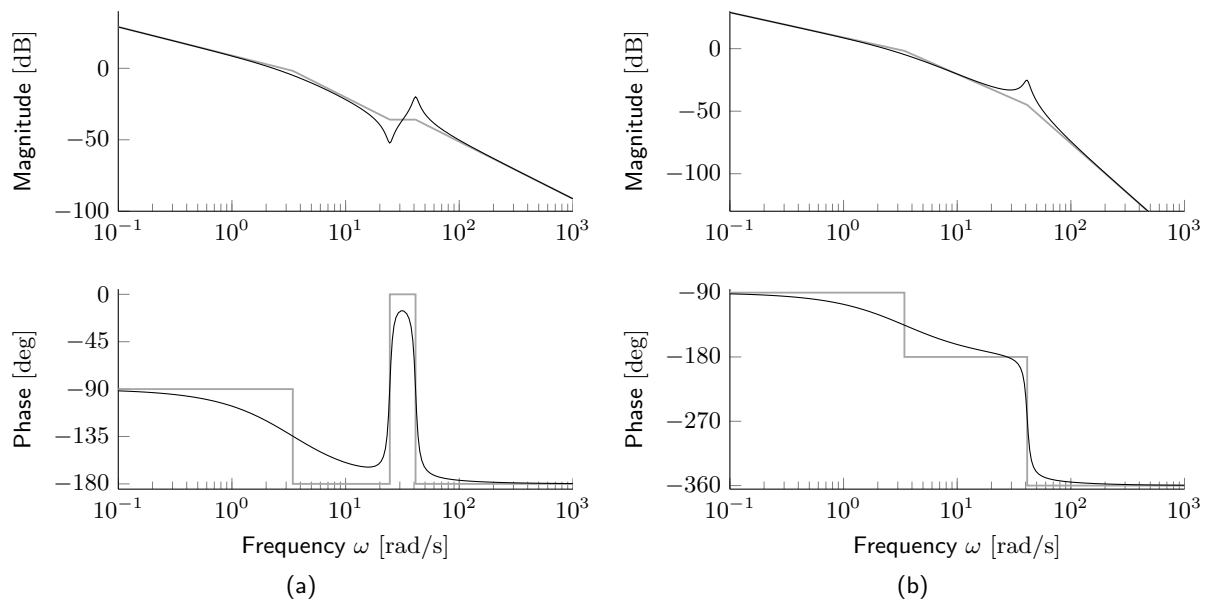

Figure 6: Bode plots of the collocated and non–collocated systems: (a) collocated system $P_{u \to \vartheta_h}(s)$; (b) non–collocated system $P_{u \to \vartheta_b}(s)$.

---

[2]An ideal situation with no actuator limitations is considered here. In practice, note that a too high crossover frequency usually requires a large control effort, that could saturate the actuator. In this circumstance, the closed–loop system could become unstable.
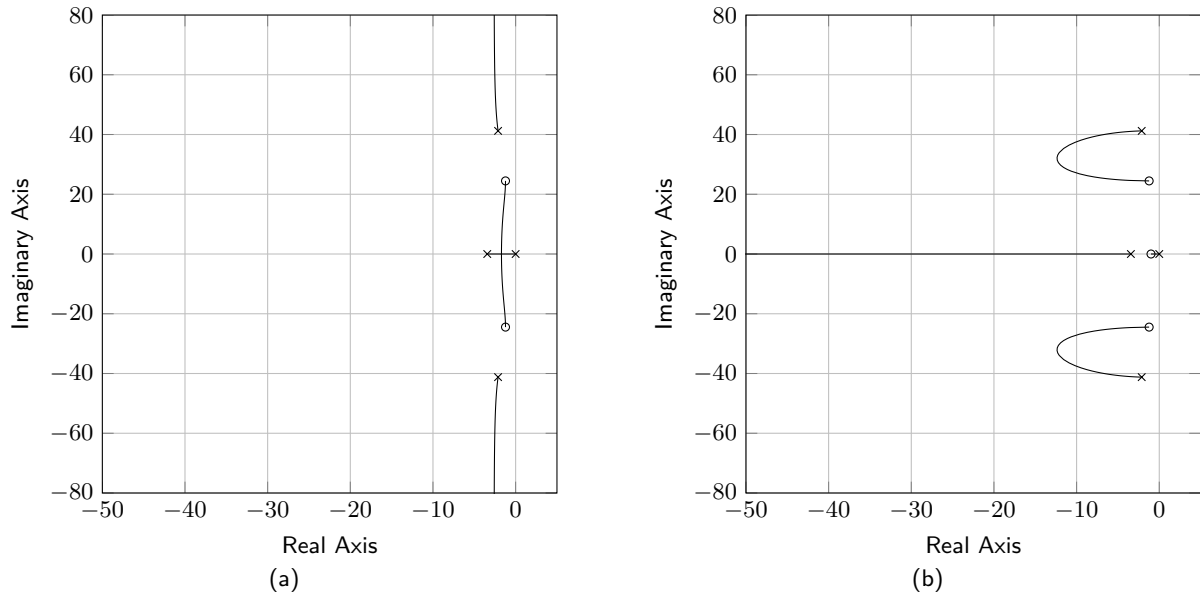
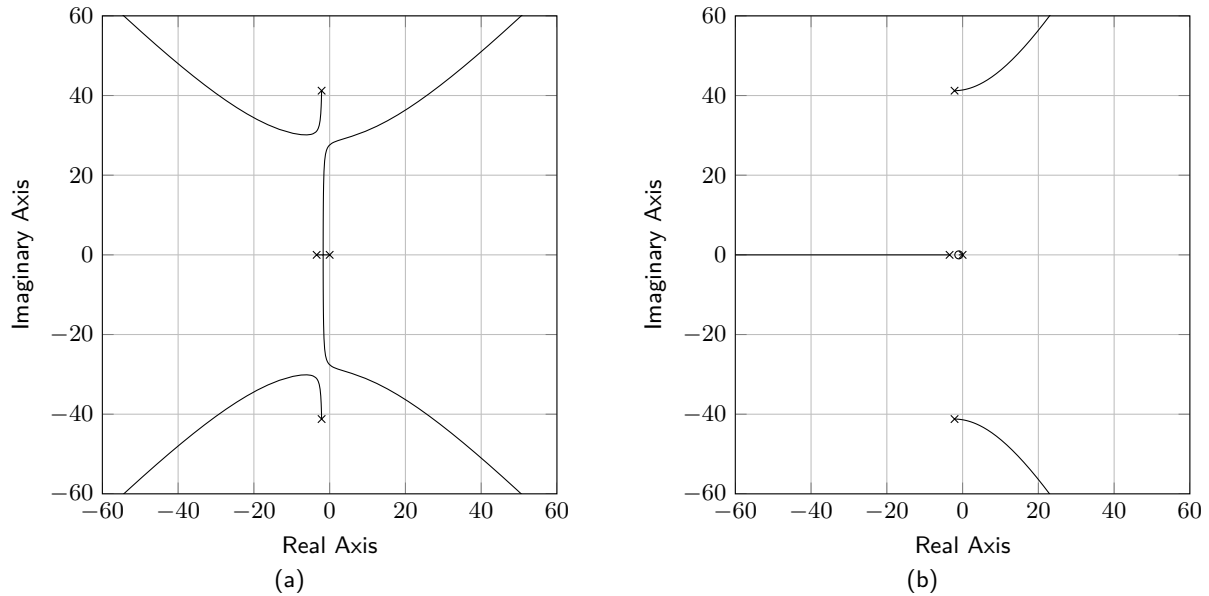Figure 7: Root loci for collocated control: (a) with P compensation; (b) with PD compensation.

Figure 8: Root loci for non–collocated control: (a) with P compensation; (b) with PD compensation.

The gain–stabilization method is exemplified in Fig. 9 for the case of a P compensation. Say M_r the magnitude of the resonant peak of the plant transfer function. Then, if $K_p \leq 1/M_r$, as in Fig. 9a and 9b, there is no encirclement of the critical point and the closed–loop system is stable. When K_p is slightly larger than $1/M_r$, as in the case of Fig. 9c, there are multiple crossings of the unit circle, but yet no encirclements of the critical point: hence, the design is still stable. However, when the K_p assumes larger values, as in Fig. 9d, the Nyquist plot encircles the critical point, and the closed–loop system becomes unstable.

The case of a PD compensation is shown in Fig. 10. Say M_r' the magnitude of the resonant peak of the loop transfer function with unit gain K_p. Then, if $K_p \leq 1/M_r'$, as shown in Fig. 10a, there is no encirclement of the critical point and the closed–loop system is stable. However, when $K_p \geq 1/M_r'$, as in Fig. 10b, the Nyquist plot encircles the critical point, and the closed–loop system becomes

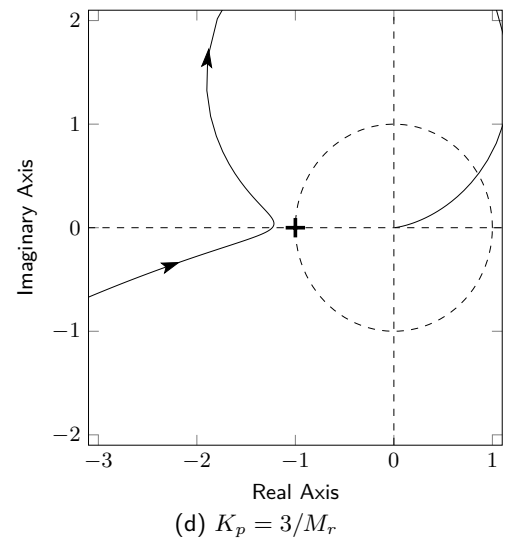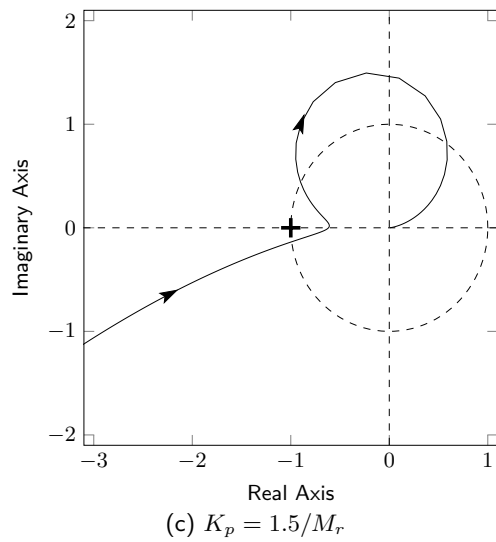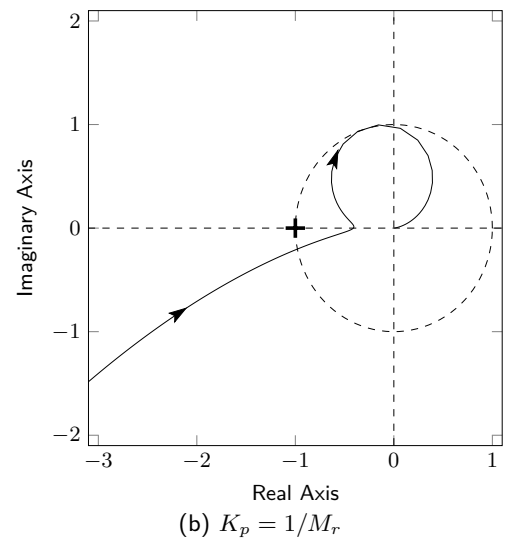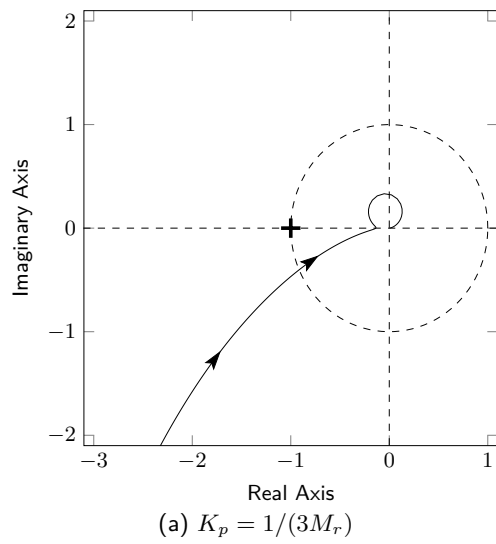(a) $K_p = 1/(3M_r)$

(b) $K_p = 1/M_r$

(c) $K_p = 1.5/M_r$

(d) $K_p = 3/M_r$

Figure 9: Nyquist plots for non–collocated control with P compensation.
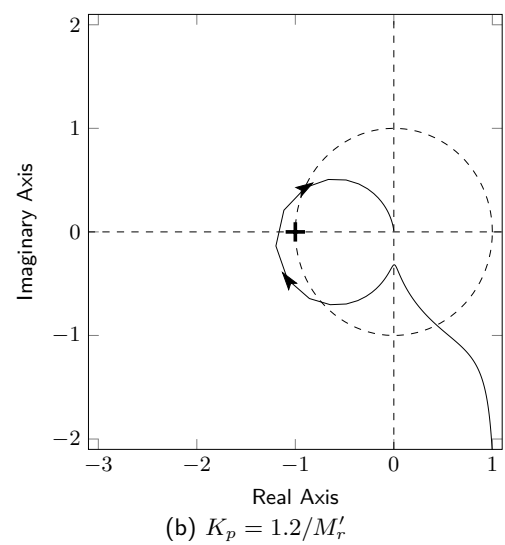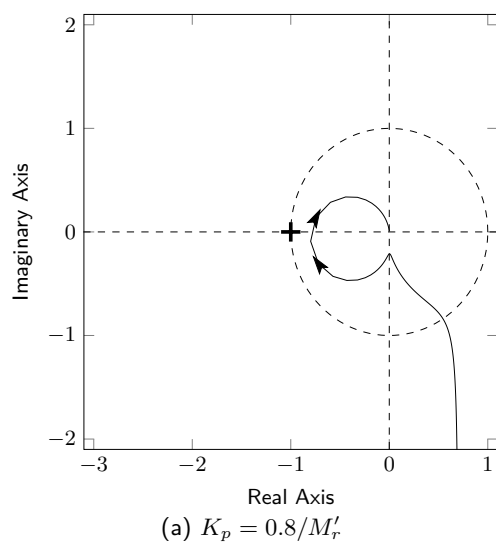
(a) $K_p = 0.8/M_r'$

(b) $K_p = 1.2/M_r'$

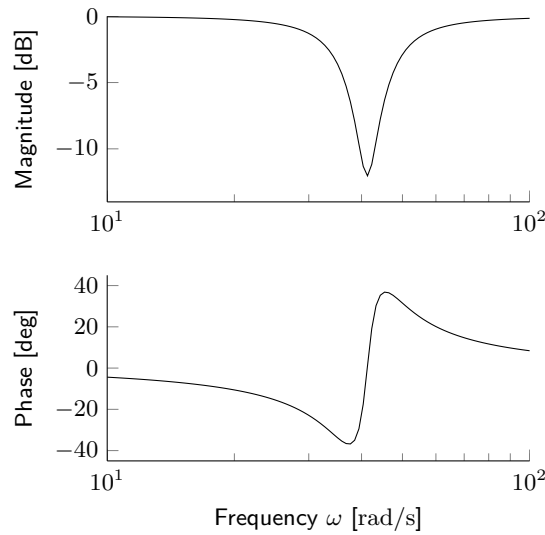Figure 10: Nyquist plots for non–collocated control with PD compensation.

Figure 11: Bode plot of the notch filter (85) used for gain stabilization.

unstable.

A more sophisticated gain stabilized design can be performed by using a *notch filter*, which allows to introduce a localised gain attenuation over a narrow frequency range. To illustrate a gain stabilized design based on notch filtering, reconsider the non–collocated control design with PD compensation of Fig. 10b. The Nyquist plot of the loop transfer function is repeated in Fig. 12a, together with the Bode plot of Fig. 12b. The design is obviously unstable. By adding the notch filter

$$C_n(s) = \frac{s^2 + 2\,\delta_z\,\omega_p\,s + \omega_p^2}{s^2 + 2\,\delta_p\,\omega_p\,s + \omega_p^2} \qquad \text{with} \qquad \delta_z = 0.05\,, \quad \delta_p = 0.2 \tag{85}$$

to the PD compensator, the situation changes as shown in Fig. 12c and 12d. The Bode plot of the notch filter is shown in Fig. 11. The design is now stable, with very large stability margins. Thanks to the large gain margin, it is possible to increase the DC gain, without compromising the stability, in order to achieve a larger control bandwidth (i.e. larger gain crossover frequency). The new design with a three times larger DC gain is shown in Fig. 12e and 12f.

In practice, the notch filter prevents the control signal of exciting the resonant mode. However, since the resonant mode is not modified by the feedback, a load disturbance can still excite the resonance, and hence can produce large oscillation at the plant output. This fact represents the main limitation of the notch filter compensation. Another limitation is that the design of the notch compensator requires a very good knowledge of the resonance amplitude and frequency, namely an information that is typically difficult to obtain.

- *Phase stabilization method* (or *phase–stabilized design*): the stability is achieved by modifying the phase of the frequency response around the resonance frequency, in order to avoid the encirclements of the critical point -1 in the Nyquist plot. In this way, stability can be achieved even if the frequency response magnitude exceeds the unit level at high frequency. In principle, higher gain crossover frequencies (and hence higher control bandwidths) can be achieved with a phase–stabilized design; unfortunately, the methods requires a good knowledge of the of the resonance peak and frequency, which rarely happens in practice. Compared to gain–stabilization, the phase–stabilization is hence more sensitive to errors in the plant model used for the compensator design.
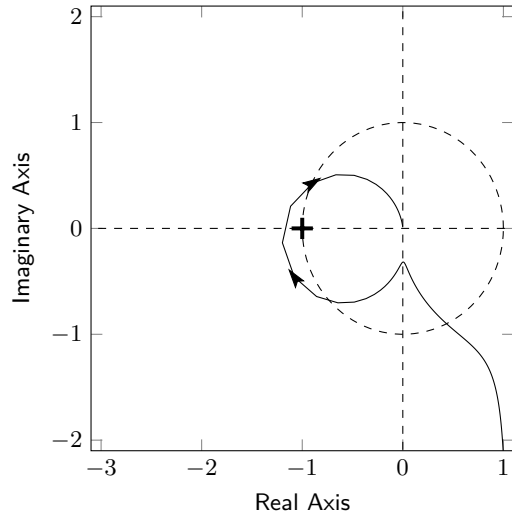
(a) $K_p = 1.2/M_r'$
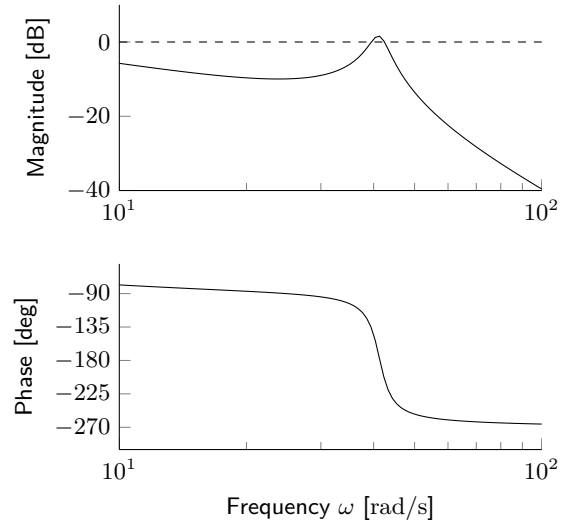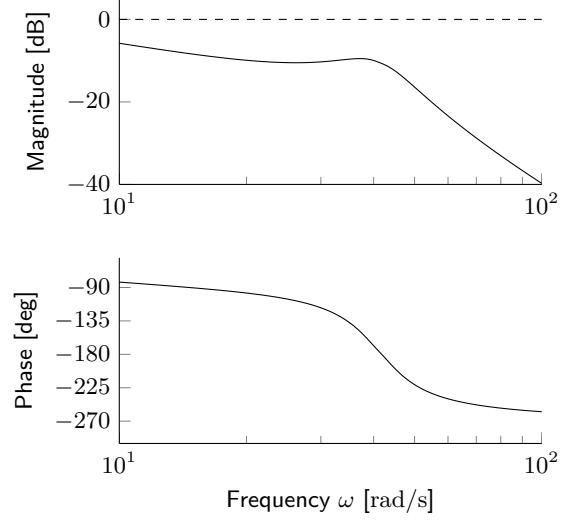
(b) $K_p = 1.2/M_r'$
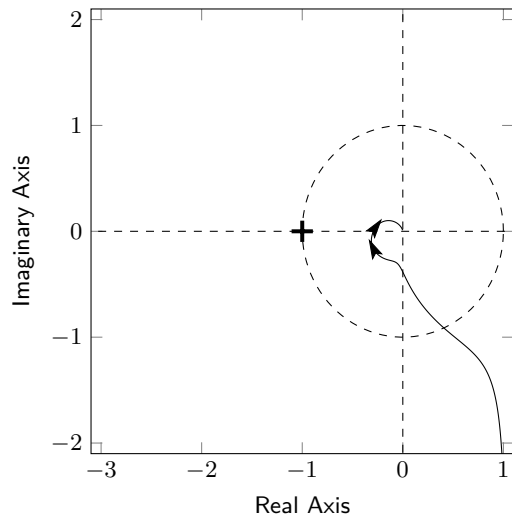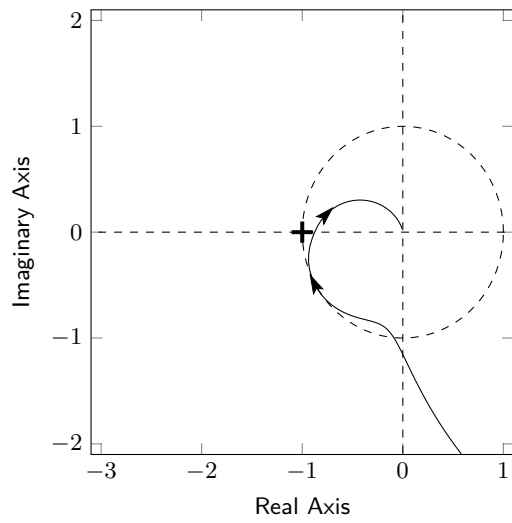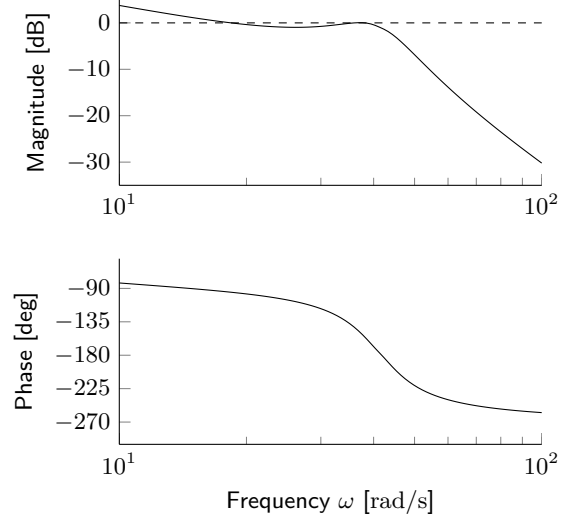
(c) $K_p = 1.2/M_r'$ + notch–pass filter

(d) $K_p = 1.2/M_r'$ + notch–pass filter

(e) $K_p = 3.6/M_r'$ + notch–pass filter

(f) $K_p = 3.6/M_r'$ + notch–pass filter

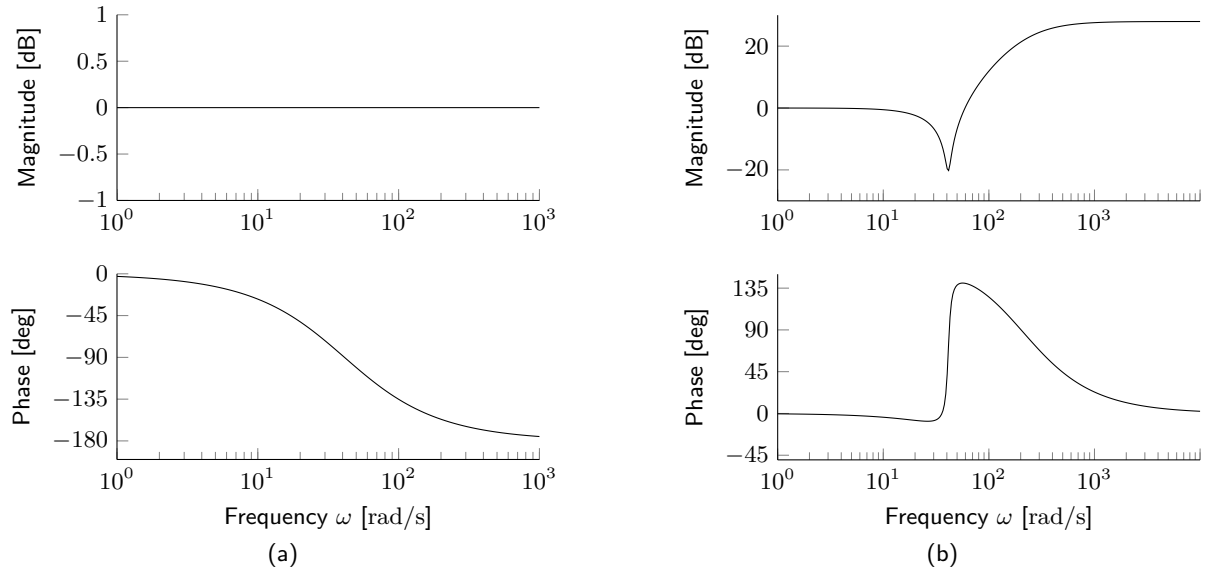Figure 12: Gain stabilized design with PD compensation and notch filter.

Figure 13: Bode plots of the two filters used for phase stabilization: (a) all–pass filter (86); (b) notch filter (87).

Phase–stabilization is typically performed with an *all–pass* or *notch* filters. Other useful compensators for phase–stabilization are the *complex lead–lag compensators* (i.e. lead–lag compensators with resonant pole–zero pairs[3]), which are however not considered in this course.

To clarify the concept of phase stabilization, reconsider the non–collocated control design with PD compensation of Fig. 10b. The Nyquist and Bode plots of plot of the loop transfer function are repeated in Fig. 14a and Fig. 14b. Consider to add the following *all–pass* filter

$$C_a(s) = \frac{-s + \omega_p}{s + \omega_p} \tag{86}$$

to the PD compensator. The Bode plot of such filter is shown in Fig. 13a. The effect of the all–pass filter is that of producing a clockwise rotation of the resonant lobe in the Nyquist plot, as shown in Fig. 14c. Thanks to the clockwise rotation, the Nyquist plot is moved away of the critical point, and the gain margin is increased. Since there are no encirclements of the critical point, the design is stable, even if there are multiple crossings of the 0–dB line in the Bode magnitude plot (see Fig. 14d). Note that the increased gain margin allows to increase the proportional gain K_p, as shown in Fig. 14e, which in turn produces an increased control bandwidth (gain cross–over frequency).

An alternative phase stabilized design can be obtained by using a notch filter of the type

$$C_n(s) = \frac{s^2 + 2\,\delta_z\,\omega_p\,s + \omega_p^2}{(1 + s/\omega_0)^2} \qquad \text{with} \qquad \delta_z = 0.05\,, \quad \omega_0 = 5\,\omega_p \tag{87}$$

whose Bode plot is shown in Fig. 13b. In this case, the notch filter is not used for introducing a localised gain attenuation, as for the gain stabilization case, but instead to introduce a large phase lead around the resonance frequency. The phase lead produces an counter–clockwise rotation of the resonant lobe in the Nyquist plot, as shown in Fig. 15c (note that different from the all–pass filter, the notch filter also attenuates the resonant peak). Thanks to the clockwise rotation, the Nyquist plot is

---

[3]W.C. Messner, M.D. Bedillion, L. Xia and D.C. Karns, "Lead and lag compensators with complex poles and zeros: design formulas for modeling and loop shaping," in IEEE Control Systems, vol. 27, no. 1, pp. 44–54, Feb. 2007.
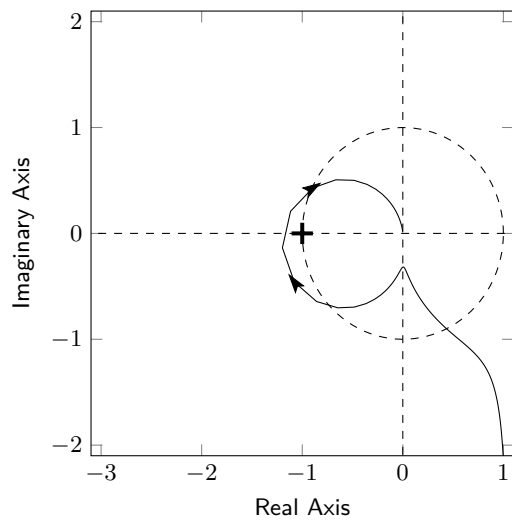
(a) $K_p = 1.2/M'_r$
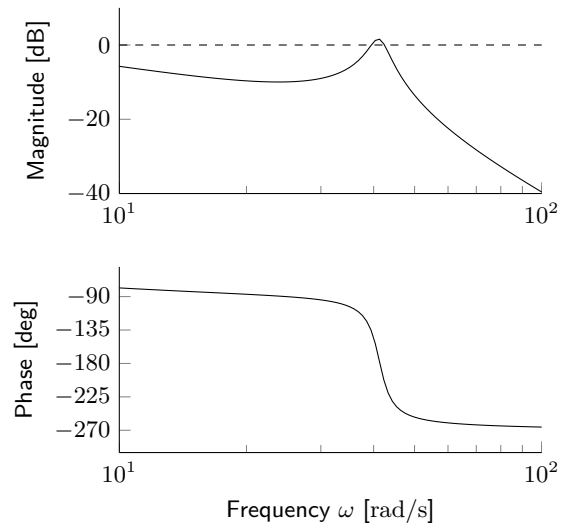
(b) $K_p = 1.2/M'_r$
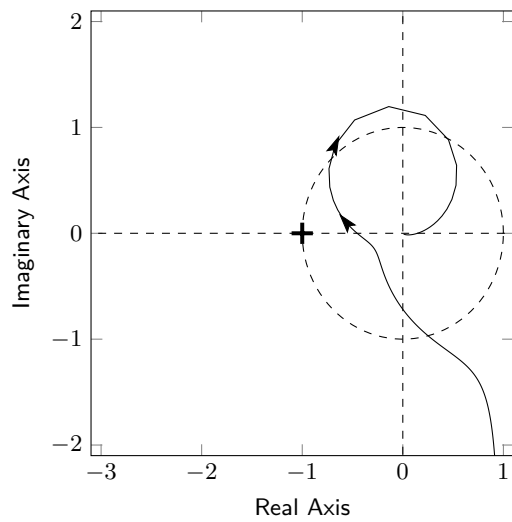
(c) $K_p = 1.2/M'_r$ + all–pass filter
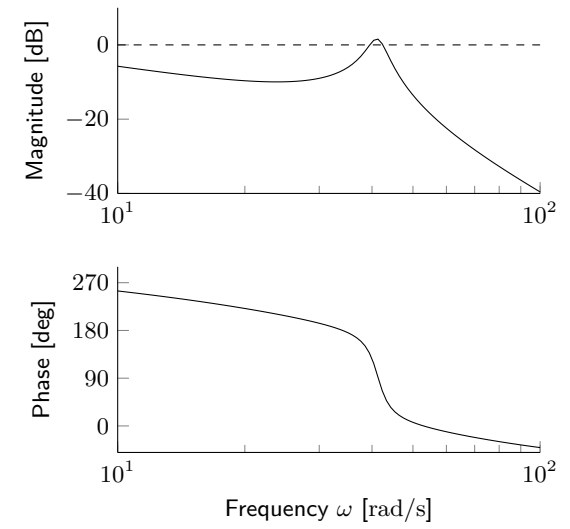
(d) $K_p = 1.2/M'_r$ + all–pass filter
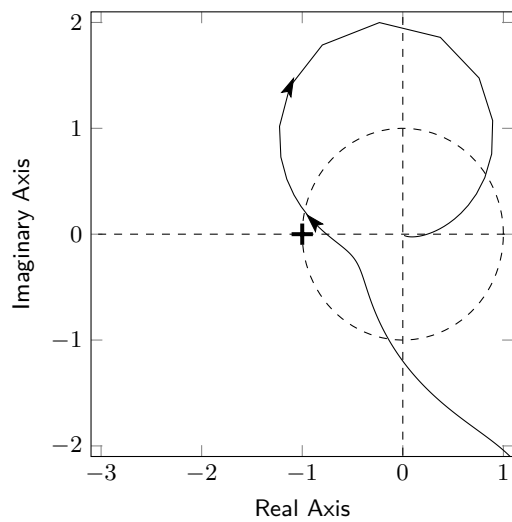
(e) $K_p = 2.0/M'_r$ + all–pass filter
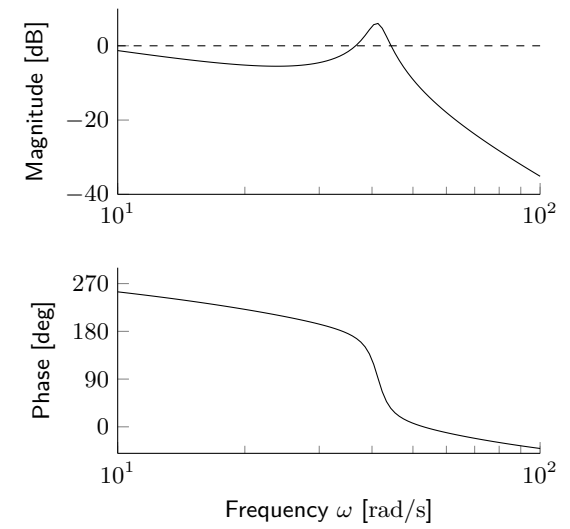
(f) $K_p = 2.0/M'_r$ + all–pass filter

Figure 14: Phase stabilized design with PD compensation and all–pass filter.

(a) $K_p = 1.2/M_r'$

(b) $K_p = 1.2/M_r'$

(c) $K_p = 1.2/M_r'$ + notch filter

(d) $K_p = 1.2/M_r'$ + notch filter

(e) $K_p = 12/M_r'$ + notch filter

(f) $K_p = 12/M_r'$ + notch filter

Figure 15: Phase stabilized design with PD compensation and notch filter.

moved away of the critical point, and the gain margin is increased. Since there are no encirclements of the critical point, the design is stable. Due to the large gain margin, the proportional gain K_p of the PD compensator can be increased, as shown in Fig. 15e and Fig. 15f, in order to achieve a larger gain crossover frequency, and hence an improved control bandwidth.

7 State–space control design using LQR methods

All the state–space control methods introduced in laboratory activity 1 for the DC gearmotor with inertial load can be immediately applied to the control of the DC gearmotor with the resonant load. The state feedback matrix $\boldsymbol{K}$ (state feedback controller gain) can be determined by a conventional (controller) eigenvalues placement procedure, as done in the laboratory activity 1. Alternatively, the matrix can be designed by resorting to linear quadratic (LQ) optimal design methods, as illustrated in the following.

7.1 LQ optimal control problem

The steady–state (or infinite horizon) linear quadratic (LQ) optimal control problem for a *continuous–time* linear, time–invariant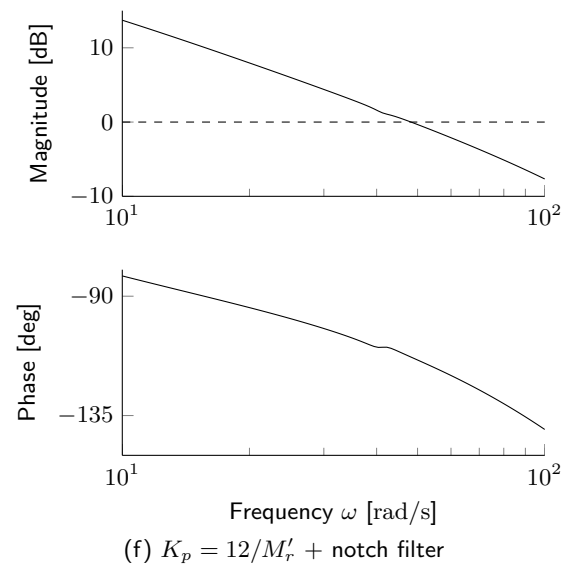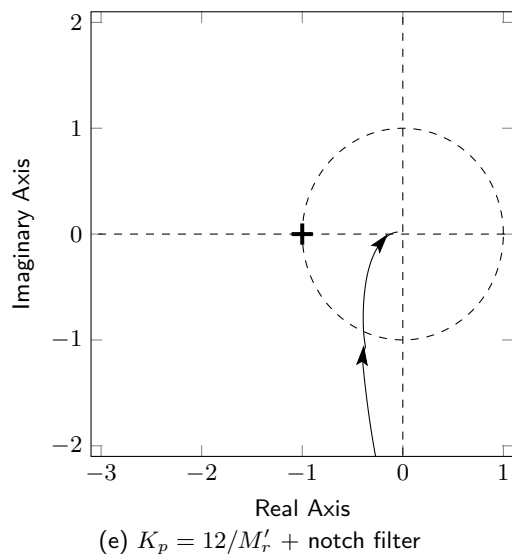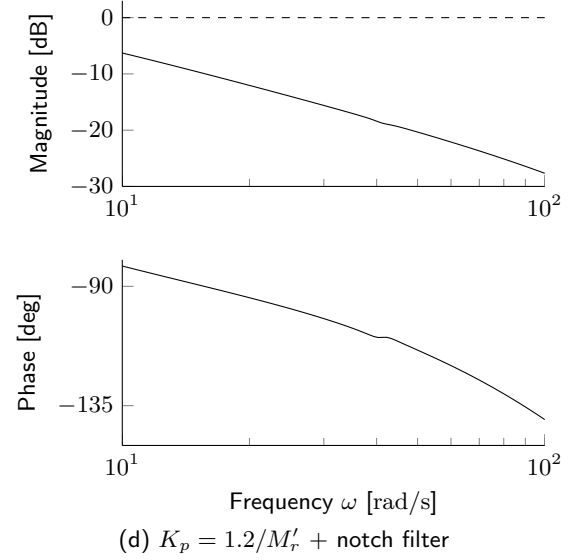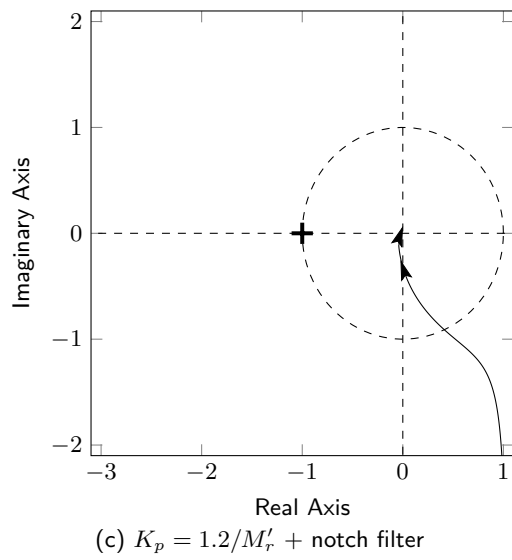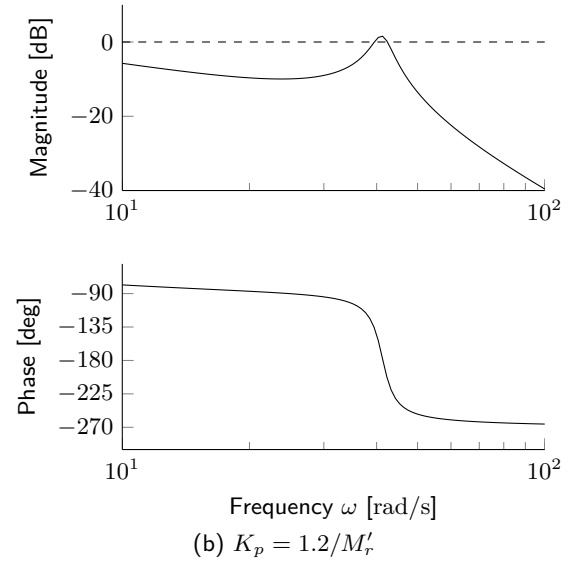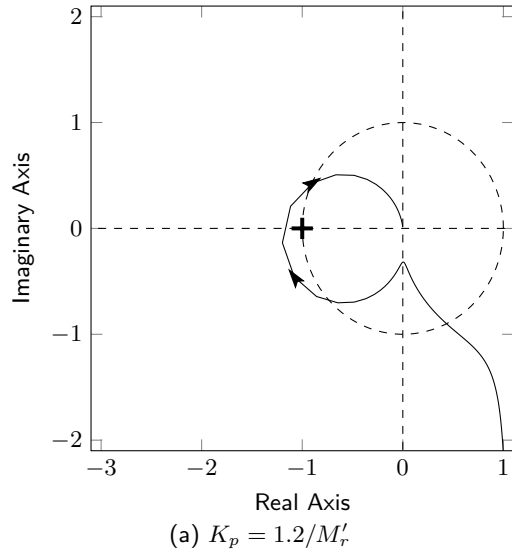 (LTI) state–space model $\Sigma = (\boldsymbol{A}, \boldsymbol{B}, \boldsymbol{C}, \boldsymbol{D})$ is formulated as follows:

Problem 1 (*Infinite horizon LQ optimal control problem*)**.**
Find the control input $\boldsymbol{u}(t)$ with $t \in [0, +\infty)$ that solves the following optimisation problem:

$$\text{minimise} \quad J \;=\; \int_0^{+\infty} \boldsymbol{x}^T(t)\,\boldsymbol{Q}\,\boldsymbol{x}(t) \;+\; \boldsymbol{u}^T(t)\,\boldsymbol{R}\,\boldsymbol{u}(t)\,dt \tag{88}$$

$$\text{subject to} \quad \dot{\boldsymbol{x}} \;=\; \boldsymbol{A}\,\boldsymbol{x} \;+\; \boldsymbol{B}\,\boldsymbol{u} \tag{89}$$

where the cost *cost weights* $\boldsymbol{Q}$ and $\boldsymbol{R}$ in the quadratic *cost function* (*performance index*) (88) are chosen such that $\boldsymbol{Q} \geq 0$ (positive semidefinite matrix) and $\boldsymbol{R} > 0$ (positive definite matrix). $\quad\square$

The criteria (88) penalizes all the state and input deviations from the equilibrium state at the origin. Therefore, the resulting control law will be a *regulator* that tries to keep the state and input variables as close to the origin as possible, according to the selection of the cost weights. This observation motivates the usage of the acronym LQR (Linear Quadratic Regulator) to denote the control law that minimises the cost (88).

When dealing with problems related to tracking of constant reference signals (set–points), the state and input values could be different to zero at steady–state. Hence, it makes sense to rewrite the cost (88) to penalize the deviations from the steady–state values, instead from the origin. Denote with $\boldsymbol{x}_\infty$ and $\boldsymbol{u}_\infty$ the values reached at steady–state by the state and input variables, i.e.

$$\boldsymbol{x}_\infty \;=\; \lim_{t \to +\infty} \boldsymbol{x}(t)\,, \qquad \boldsymbol{u}_\infty \;=\; \lim_{t \to +\infty} \boldsymbol{u}(t) \tag{90}$$

Then, the new cost function can be specified as follows

$$J' \;=\; \int_0^{+\infty} (\boldsymbol{x}(t) - \boldsymbol{x}_\infty)^T \,\boldsymbol{Q}\,(\boldsymbol{x}(t) - \boldsymbol{x}_\infty) \;+\; (\boldsymbol{u}(t) - \boldsymbol{u}_\infty)^T \,\boldsymbol{R}\,(\boldsymbol{u}(t) - \boldsymbol{u}_\infty)\,dt \tag{91}$$

The problem of minimising (91) subject to the plant dynamics

$$\dot{\boldsymbol{x}} \; = \; \boldsymbol{A}\,\boldsymbol{x} \; + \; \boldsymbol{B}\,\boldsymbol{u} \tag{92}$$

can be reformulated as a conventional LQR problem in the new state and input variables

$$\boldsymbol{x}_\delta \; = \; \boldsymbol{x} - \boldsymbol{x}_\infty, \qquad \boldsymbol{u}_\delta \; = \; \boldsymbol{u} - \boldsymbol{u}_\infty \tag{93}$$

that represent the deviations from the steady–state values. In fact, in the new variables, the cost function (91) can be rewritten as follows

$$J' \; = \; \int_0^{+\infty} \boldsymbol{x}_\delta^T(t)\,\boldsymbol{Q}\,\boldsymbol{x}_\delta(t) \; + \; \boldsymbol{u}_\delta^T(t)\,\boldsymbol{R}\,\boldsymbol{u}_\delta(t)\,dt \tag{94}$$

Moreover, the original plant dynamics (92) becomes

$$\dot{\boldsymbol{x}} \; = \; \boldsymbol{A}\,\boldsymbol{x} \; + \; \boldsymbol{B}\,\boldsymbol{u} \quad \xrightarrow{\substack{\boldsymbol{x}=\boldsymbol{x}_\delta+\boldsymbol{x}_\infty \\ \boldsymbol{u}=\boldsymbol{u}_\delta+\boldsymbol{u}_\infty}} \quad \dot{\boldsymbol{x}}_\delta \; = \; \boldsymbol{A}\,\boldsymbol{x}_\delta \; + \; \boldsymbol{B}\,\boldsymbol{u}_\delta \; + \; \underbrace{(\boldsymbol{A}\,\boldsymbol{x}_\infty + \boldsymbol{B}\,\boldsymbol{u}_\infty)}_{\dot{\boldsymbol{x}}_\infty=0} \tag{95}$$

Hence, the problem of minimising (91) subject to the original plant dynamics (92) is recast as a conventional LQR problem with cost (94) and plant dynamics (95).

Regarding the design of the LQR, the following result holds:

Theorem 1 (*solution of the infinite horizon LQ optimal control problem*)**.**
Let $\sqrt{\boldsymbol{Q}}$ be a matrix such that $\boldsymbol{Q} = \sqrt{\boldsymbol{Q}}^T \sqrt{\boldsymbol{Q}}$. It holds that:

1. the *Algebraic Riccati Equation* (ARE):

$$\boldsymbol{A}^T\boldsymbol{P} \; + \; \boldsymbol{P}\boldsymbol{A} \; - \; \boldsymbol{P}\boldsymbol{B}\boldsymbol{R}^{-1}\boldsymbol{B}^T\boldsymbol{P} \; + \; \boldsymbol{Q} \; = \; \boldsymbol{0} \tag{96}$$

   has a *unique* positive semidefinite solution $\boldsymbol{P}_\infty$.

   Moreover, if $(\boldsymbol{A},\,\sqrt{\boldsymbol{Q}})$ is observable, then $\boldsymbol{P}_\infty$ is positive definite.

2. the state feedback control law:

$$\boldsymbol{u}(t) \; = \; -\boldsymbol{K}\,\boldsymbol{x}(t) \qquad \text{with} \qquad \boldsymbol{K} \; = \; \boldsymbol{R}^{-1}\boldsymbol{B}^T\boldsymbol{P}_\infty \tag{97}$$

   minimises the infinite horizon quadratic cost function (88), and makes the closed–loop system asymptotically stable.

if and only if $(\boldsymbol{A},\,\boldsymbol{B})$ is *stabilizable* and $(\boldsymbol{A},\,\sqrt{\boldsymbol{Q}})$ is *detectable*. $\qquad\qquad$ □

The LQR problem can be generalised to include the combined input–state weighing term $\boldsymbol{u}^T\boldsymbol{N}\boldsymbol{x}$ in the cost function. This generalisation is useful to solve certain LQR–related problems, such as the LQR with frequency dependent weights (frequency–shaped LQR).

Problem 2 (*Infinite horizon LQ optimal control problem with generalised cost*).
Find the control input $\boldsymbol{u}(t)$ with $t \in [0, +\infty)$ that solves the following optimisation problem:

$$\text{minimise} \quad J = \int_0^{+\infty} \begin{bmatrix} \boldsymbol{x}^T & \boldsymbol{u}^T \end{bmatrix} \begin{bmatrix} \boldsymbol{Q} & \boldsymbol{N} \\ \boldsymbol{N}^T & \boldsymbol{R} \end{bmatrix} \begin{bmatrix} \boldsymbol{x} \\ \boldsymbol{u} \end{bmatrix} dt \tag{98}$$

$$\text{subject to} \quad \dot{\boldsymbol{x}} = \boldsymbol{A}\,\boldsymbol{x} + \boldsymbol{B}\,\boldsymbol{u} \tag{99}$$

where the cost *cost weights* $\boldsymbol{Q}$ and $\boldsymbol{R}$ in (98) are chosen such that $\boldsymbol{Q} \geq 0$ (positive semidefinite matrix) and $\boldsymbol{R} > 0$ (positive definite matrix). □

It can be proved that the generalised LQR problem 2 can be reduced to the following LQR problem with standard cost:

$$\text{minimise} \quad J = \int_0^{+\infty} \boldsymbol{x}^T(t)\,\tilde{\boldsymbol{Q}}\,\boldsymbol{x}(t) + \boldsymbol{v}^T(t)\,\boldsymbol{R}\,\boldsymbol{v}(t)\,dt \tag{100}$$

$$\text{subject to} \quad \dot{\boldsymbol{x}} = \left(\boldsymbol{A} - \boldsymbol{B}\boldsymbol{R}^{-1}\boldsymbol{N}^T\right)\boldsymbol{x} + \boldsymbol{B}\,\boldsymbol{v} \tag{101}$$

where

$$\tilde{\boldsymbol{Q}} = \boldsymbol{Q} - \boldsymbol{N}\boldsymbol{R}^{-1}\boldsymbol{N}^T \quad \text{and} \quad \boldsymbol{v} = \boldsymbol{u} + \boldsymbol{R}^{-1}\boldsymbol{N}^T\boldsymbol{x} \tag{102}$$

Based on this fact, the Thm. 1 can be easily generalised to solve the problem 2:

Theorem 2 (*solution of the infinite horizon LQ optimal control problem with generalised cost*).
Assume that $\tilde{\boldsymbol{Q}} \geq 0$, and denote with $\sqrt{\tilde{\boldsymbol{Q}}}$ a matrix such that $\tilde{\boldsymbol{Q}} = \sqrt{\tilde{\boldsymbol{Q}}}^T \sqrt{\tilde{\boldsymbol{Q}}}$. It holds that:

1. the *Algebraic Riccati Equation* (ARE):

$$\left(\boldsymbol{A} - \boldsymbol{B}\boldsymbol{R}^{-1}\boldsymbol{N}^T\right)^T \boldsymbol{P} + \boldsymbol{P}\left(\boldsymbol{A} - \boldsymbol{B}\boldsymbol{R}^{-1}\boldsymbol{N}^T\right) - \boldsymbol{P}\boldsymbol{B}\boldsymbol{R}^{-1}\boldsymbol{B}^T\boldsymbol{P} + \tilde{\boldsymbol{Q}} = \boldsymbol{0} \tag{103}$$

   has a *unique* positive semidefinite solution $\boldsymbol{P}_\infty$.

   Moreover, if $(\boldsymbol{A}, \sqrt{\boldsymbol{Q}})$ is observable, then $\boldsymbol{P}_\infty$ is positive definite.

2. the state feedback control law:

$$\boldsymbol{u}(t) = -\boldsymbol{K}\,\boldsymbol{x}(t) \quad \text{with} \quad \boldsymbol{K} = \boldsymbol{R}^{-1}\left(\boldsymbol{B}^T\boldsymbol{P}_\infty + \boldsymbol{N}^T\right) \tag{104}$$

   minimises the infinite horizon quadratic cost function (98), and makes the closed–loop system asymptotically stable.

if and only if $\left(\boldsymbol{A} - \boldsymbol{B}\boldsymbol{R}^{-1}\boldsymbol{N}^T, \boldsymbol{B}\right)$ is *stabilizable* and $\left(\boldsymbol{A} - \boldsymbol{B}\boldsymbol{R}^{-1}\boldsymbol{N}^T, \sqrt{\tilde{\boldsymbol{Q}}}\right)$ is *detectable*. □

In Matlab, the computation of the LQR gain matrix $\boldsymbol{K}$ for a problem with either standard or generalised cost is performed by the `lqr` routine.

7.2 Cost weights selection criteria

Below are reported some simple guidelines for the selection of the cost weights $\boldsymbol{Q}$ and $\boldsymbol{R}$ in the performance index (88):

1) in absence of information regarding the coupling of the state and/or input variables, select $\boldsymbol{Q}$ and $\boldsymbol{R}$ as diagonal matrices.

2) choose a large value for any diagonal element whose associated variable (either a state or control component) should be kept small, i.e. close to zero as much as possible.

Note: if all the diagonal entries of $\boldsymbol{Q}$ are chosen greater than zero, then $\sqrt{\boldsymbol{Q}}$ has full rank, and therefore $(\boldsymbol{A}, \sqrt{\boldsymbol{Q}})$ is detectable.

3) only "relative" values are relevant in the weights selection: increasing the elements of both $\boldsymbol{Q}$ and $\boldsymbol{R}$ by the same factor produces no effect on the optimal solution.

In particular, the choice of $\boldsymbol{Q}$ and $\boldsymbol{R}$ is a trade–off between the *control effort* $\int_0^{+\infty} \boldsymbol{u}^T \boldsymbol{R} \boldsymbol{u} \, dt$ (i.e. input energy) and the *control accuracy* $\int_0^{+\infty} \boldsymbol{x}^T \boldsymbol{Q} \boldsymbol{x} \, dt$ (i.e. regulation error energy).

4) let $\bar{x}_i$ and $\bar{u}_i$ denote the maximum acceptable deviations of the ith component of the state and input vectors, respectively. A tentative choice for $\boldsymbol{Q}$ and $\boldsymbol{R}$ can be the following (*Bryson's rule*):

$$
\begin{aligned}
\boldsymbol{Q} &= \operatorname{diag}\{q_{ii}\}_{i=1,\,...,\,n} & \text{with} \qquad q_{ii} &= \frac{1}{\bar{x}_i^2} \\[2mm]
\boldsymbol{R} &= \operatorname{diag}\{r_{ii}\}_{i=1,\,...,\,m} & \text{with} \qquad r_{ii} &= \frac{1}{\bar{u}_i^2}
\end{aligned}
\tag{105}
$$

where diag denotes a diagonal matrix with specified elements on the leading diagonal. Starting from this initial choice, some small adjustments (using "trial and error") may be required to finally obtain a satisfactory closed–loop response.

Sometimes, an extra factor ρ is included in the definition of $\boldsymbol{R}$ reported in (105), namely $\boldsymbol{R} = \rho \operatorname{diag}\{r_{ii}\}$, to consider the relative weighting between the control input and control error energies.

7.3 Location of LQR eigenvalues

In general, there is no direct control over the locations of the controller eigenvalues generated by an LQR design. However, the eigenvalue placement can be somehow driven through suitable choices of the cost weights or the plant model. Below are reported some options:

1) It is possible to design a LQR with a *prescribed deegree of stability*, namely a state–space controller whose eigenvalues have real part less than a specified negative value $-\alpha$.

For the design, the following fact from linear algebra is used:

$$
\Re \lambda_i \left(\boldsymbol{A} - \boldsymbol{B}\boldsymbol{K}\right) < -\alpha \qquad \Leftrightarrow \qquad \Re \lambda_i \left((\boldsymbol{A} + \alpha \boldsymbol{I}) - \boldsymbol{B}\boldsymbol{K}\right) < 0
\tag{106}
$$

where $\Re$ denotes the real part of a complex number, and λ_i denotes the ith eigenvalue of the specified matrix. From (106), it follows that the design of an LQR with a degree of stability α for the plant model (92) is equivalent to the design of a standard LQR that asymptotically stabilizes the plant dynamics

$$
\dot{\boldsymbol{x}} = (\boldsymbol{A} + \alpha \boldsymbol{I})\,\boldsymbol{x} + \boldsymbol{B}\,\boldsymbol{u}
\tag{107}
$$

Note that in an LQR design with degree of stability α, all the modes of the closed–loop system dynamics decay faster than the exponential $e^{\alpha t}$. In this sense, the LQR design with a prescribed degree of stability is equivalent to a design for a prescribed exponential decaying rate of the closed–loop modes.

2) It is possible to design a LQR whose eigenvalue lie in a disk with centre in $(-\alpha, 0)$ and radius $0 < \rho < \alpha$. This is useful to specify certain limits on the damping ratio of the closed–loop poles, in addition to the convergence rate to zero.

The design relies on solving an auxiliary discrete–time LQR problem for the plant model

$$\boldsymbol{x}[k+1] \;=\; \tfrac{1}{\rho}\,(\boldsymbol{A}\,+\,\alpha\,\boldsymbol{I})\,\boldsymbol{x}[k] \;+\; \tfrac{1}{\rho}\,\boldsymbol{B}\,\boldsymbol{u}[k] \tag{108}$$

with the same cost weights of the original continuous–time LQR problem.

Since the discrete–time LQR is designed to yield an asymptotically stable closed–loop system, it follows that all the closed–loop eigenvalues lie within the unit circle, i.e.

$$\left| \lambda_i\left(\tfrac{1}{\rho}\,(\boldsymbol{A}\,+\,\alpha\,\boldsymbol{I}\,-\,\boldsymbol{B}\boldsymbol{K}) \right) \right| \;<\; 1 \tag{109}$$

where λ_i denotes the ith eigenvalue of the specified matrix. Then, by using the following equivalences

$$\left| \lambda_i\left(\tfrac{1}{\rho}\,(\boldsymbol{A}\,+\,\alpha\,\boldsymbol{I}\,-\,\boldsymbol{B}\boldsymbol{K}) \right) \right| \;<\; 1 \qquad \Leftrightarrow \qquad |\,\lambda_i\,(\boldsymbol{A}\,+\,\alpha\,\boldsymbol{I}\,-\,\boldsymbol{B}\boldsymbol{K}\,)\,| \;<\; \rho$$

$$\Leftrightarrow \qquad |\,\lambda_i\,(\boldsymbol{A}\,-\,\boldsymbol{B}\boldsymbol{K}\,)\,+\,\alpha\,| \;<\; \rho \tag{110}$$

it follows that the eigenvalues of the matrix $\boldsymbol{A} - \boldsymbol{B}\boldsymbol{K}$, which are the closed–loop eigenvalues of the continuous–time LQR with state matrix $\boldsymbol{K}$, lie within the circle with centre $-\alpha$ and radius ρ.

3) For the following LQR problem:

$$\text{minimise} \quad J = \int_0^{+\infty} z^2(t)\,+\,r\,u^2(t)\,dt \qquad r > 0$$

$$\text{subject to} \quad \Sigma : \begin{cases} \dot{\boldsymbol{x}} \;=\; \boldsymbol{A}\,\boldsymbol{x}\,+\,\boldsymbol{B}\,u \\ z \;=\; \boldsymbol{C}\,\boldsymbol{x} \end{cases} \tag{111}$$

where both u and z are scalars (i.e. the plant is a single–input, single–output system), it is possible to exactly determine the locations of the closed–loop eigenvalues. In fact, the following result holds:

Theorem 3 (*Symmetric Root Locus*).
The closed–loop eigenvalues associated with the LQR design (111) are the stable roots of the polynomial

$$p(s) \;=\; D(-s)\,D(s)\,+\,\frac{1}{r}\,N(-s)\,N(s) \tag{112}$$

where $N(s)$ and $D(s)$ are the numerator and denominator of the input–output transfer function of the model Σ, i.e.

$$G(s) = \frac{N(s)}{D(s)} = \boldsymbol{C}\,(s\boldsymbol{I}-\boldsymbol{A})\,\boldsymbol{B} \qquad \Rightarrow \qquad \begin{aligned} N(s) &= \boldsymbol{C}\,\mathrm{adj}\,(s\boldsymbol{I}-\boldsymbol{A})\,\boldsymbol{B} \\ D(s) &= \det\,(s\boldsymbol{I}-\boldsymbol{A}) \end{aligned} \tag{113}$$

$\square$

The polynomial (112) can be regarded as the characteristic polynomial of a closed–loop system with unit feedback and loop transfer function equal to $(1/r)\,G(-s)\,G(s)$. The root locus of such feedback system, parametrised with respect to the gain r, is referred to *symmetric root locus* (SRL). As any root locus, the SRL is symmetric with respect to the real axis; however, the SRL is also symmetric with respect to the imaginary axis (hence, the name "symmetric" root locus). Let

$$D(s) \;=\; \prod_{i=1}^{n}(s - p_i)\,, \qquad N(s) \;=\; \alpha \prod_{i=1}^{m}(s - z_i) \qquad \text{with} \qquad m \le n \tag{114}$$

For sketching the root locus, the polynomial (112) is rewritten in standard form, i.e. $p(s) = A(s) + k\,B(s)$, with $A(s)$ and $B(s)$ monic polynomials, so that the root locus is defined by the equation

$$
\begin{aligned}
p(s) \;&=\; D(-s)\,D(s) + \frac{1}{r}\,N(-s)\,N(s) \\
&=\; \underbrace{\prod_{i=1}^{n}(s - p_i)\,(s + p_i)}_{\triangleq\,A(s)} + \underbrace{(-1)^{n-m}\frac{\alpha^2}{r}}_{\triangleq\,k}\;\underbrace{\prod_{i=1}^{m}(s - z_i)\,(s + z_i)}_{\triangleq\,B(s)} \;=\; 0
\end{aligned}
\tag{115}
$$

The locus to consider could be either the positive $(k > 0)$ or negative $(k < 0)$ locus, depending on which one has *no part on the imaginary axis*: in fact, under the hypotheses of Thm. 1, the LQR design produces an asymptotically stable closed–loop system for any choice of the gain $r > 0$, and therefore the SRL should have no finite portions on the imaginary axis.

The (stable portion of the) SRL allows to analyse how the closed–loop eigenvalues of a LQR design move on the complex plane as the input cost r increases from 0 up to $+\infty$. In particular, by reminding the sketching rules for a root locus, the following "extremal" cases can be highlighted:

a) when $r \to +\infty$ (*expensive control* case), the closed–loop eigenvalues approach:
  - the stable poles of $G(s)$, i.e. the roots of $D(s)$ lying in the open left–half plane (LHP)
  - the mirror images with respect to the imaginary axis of the unstable poles of $G(s)$, i.e. the roots of $D(s)$ lying in the closed right–half plane (RHP)

b) when $r \to 0^+$ (*cheap control* case)
  - m closed–loop eigenvalues (out of n) approach
    - the zeros of $G(s)$ in the open LHP
    - the mirror images with respect to the imaginary axis of the zeros of $G(s)$ in the closed RHP
  - the remaining $n - m$ closed–loop eigenvalues go to infinity along the asymptotes of the SRL that extend in the open LHP.
  Note that the SRL has $2(n - m)$ straight asymptotes that depart from the origin with slopes:

$$
\begin{aligned}
\varphi_h^{+} &= \pm\frac{(h + 1/2)\,\pi}{n - m} && \text{with} \quad h = 0, \ldots, \frac{n - m - 1}{2} \quad \text{for } (n - m) \text{ odd} \\[2mm]
\varphi_h^{-} &= \pm\frac{h\,\pi}{n - m} && \text{with} \quad h = 0, \ldots, \frac{n - m}{2} - 1 \quad \text{for } (n - m) \text{ even}
\end{aligned}
\tag{116}
$$

  The differentiation of the odd and even cases is due to the presence of the factor $(-1)^{n-m}$ in the definition of the gain k in (115).

7.4 Frequency–shaped LQ optimal control problem

In a standard LQR problem, the state and input variables are penalized uniformly in the frequency domain: in fact, thanks to the *Parseval's theorem* [4], the cost function (88) can be rewritten as follows

$$J = \int_0^{+\infty} \boldsymbol{x}^T(t)\,\boldsymbol{Q}\,\boldsymbol{x}(t) \,+\, \boldsymbol{u}^T(t)\,\boldsymbol{R}\,\boldsymbol{u}(t)\,dt$$

$$= \frac{1}{2\pi} \int_{-\infty}^{+\infty} \boldsymbol{X}^T(j\omega)\,\boldsymbol{Q}\,\boldsymbol{X}(j\omega) \,+\, \boldsymbol{U}^T(j\omega)\,\boldsymbol{R}\,\boldsymbol{U}(j\omega)\,d\omega \tag{117}$$

To account for non–uniform weighting in the frequency domain, the following extension to the standard LQR design is introduced:

$$\text{minimise} \quad J_{FS} = \frac{1}{2\pi} \int_{-\infty}^{+\infty} \boldsymbol{X}^T(j\omega)\,\boldsymbol{Q}(j\omega)\,\boldsymbol{X}(j\omega) \,+\, \boldsymbol{U}^T(j\omega)\,\boldsymbol{R}(j\omega)\,\boldsymbol{U}(j\omega)\,d\omega \tag{118}$$

$$\text{subject to} \quad \dot{\boldsymbol{x}} \,=\, \boldsymbol{A}\,\boldsymbol{x} \,+\, \boldsymbol{B}\,\boldsymbol{u} \quad \text{with} \quad \boldsymbol{x} \in \mathbb{R}^n,\ \boldsymbol{u} \in \mathbb{R}^m$$

where $\boldsymbol{Q}(j\omega) \geq 0$ and $\boldsymbol{R}(j\omega) > 0$ for any $\omega \in \mathbb{R}$. The problem of finding the control input $\boldsymbol{u}$ over $[0, +\infty)$ that solve the optimisation problem (118) is referred as the *Frequency–Shaped LQR* (FS–LQR) design problem. A FS–LQR problem can be recast as a standard LQR problem with a generalised cost function for augmented–state system, as described below:

1) Factorise the weights $\boldsymbol{Q}(j\omega)$ and $\boldsymbol{R}(j\omega)$ as follows [5]

$$\boldsymbol{Q}(j\omega) \,=\, \boldsymbol{H}_Q^*(j\omega)\,\boldsymbol{H}_Q(j\omega)\,, \qquad \boldsymbol{R}(j\omega) \,=\, \boldsymbol{H}_R^*(j\omega)\,\boldsymbol{H}_R(j\omega) \tag{119}$$

These factorisations always exist when $\boldsymbol{Q}(j\omega)$ and $\boldsymbol{R}(j\omega)$ are diagonal matrices.

Note that $\boldsymbol{H}_Q(j\omega) \in \mathbb{C}^{r \times n}$ with $r = \operatorname{rank} \boldsymbol{H}_Q = \operatorname{rank} \boldsymbol{Q} \leq n$ because $\boldsymbol{Q}(j\omega)$ is only positive semidefinite; instead, $\boldsymbol{H}_R(j\omega) \in \mathbb{C}^{m \times m}$ because $\boldsymbol{R}(j\omega)$ is positive definite.

2) Let $\Sigma_Q = (\boldsymbol{A}_Q,\,\boldsymbol{B}_Q,\,\boldsymbol{C}_Q,\,\boldsymbol{D}_Q)$ and $\Sigma_R = (\boldsymbol{A}_R,\,\boldsymbol{B}_R,\,\boldsymbol{C}_R,\,\boldsymbol{D}_R)$ be two state–space realisations of the two transfer matrices $\boldsymbol{H}_Q(s)$ and $\boldsymbol{H}_R(s)$, i.e.

$$\Sigma_Q \ : \ \begin{cases} \dot{\boldsymbol{x}}_Q \,=\, \boldsymbol{A}_Q\,\boldsymbol{x}_Q + \boldsymbol{B}_Q\,\boldsymbol{x}\,, & \boldsymbol{x}_Q \in \mathbb{R}^{n_Q} \\ \boldsymbol{y}_Q \,=\, \boldsymbol{C}_Q\,\boldsymbol{x}_Q + \boldsymbol{D}_Q\,\boldsymbol{x}\,, & \boldsymbol{y}_Q \in \mathbb{R}^{r} \end{cases} \tag{120}$$

$$\Sigma_R \ : \ \begin{cases} \dot{\boldsymbol{x}}_R \,=\, \boldsymbol{A}_R\,\boldsymbol{x}_R + \boldsymbol{B}_R\,\boldsymbol{u}\,, & \boldsymbol{x}_R \in \mathbb{R}^{n_R} \\ \boldsymbol{y}_R \,=\, \boldsymbol{C}_R\,\boldsymbol{x}_R + \boldsymbol{D}_R\,\boldsymbol{u}\,, & \boldsymbol{y}_Q \in \mathbb{R}^{m} \end{cases} \tag{121}$$

The dimensions n_Q and n_R of the state vectors $\boldsymbol{x}_Q$ and $\boldsymbol{x}_R$ depend on the transfer matrices $\boldsymbol{H}_Q(s)$ and $\boldsymbol{H}_R(s)$, and the particular state–space realisation (the realisation is, in general, not unique).

3) Using

$$\boldsymbol{Y}_Q(j\omega) \,=\, \boldsymbol{H}_Q(j\omega)\,\boldsymbol{X}(j\omega) \quad \text{and} \quad \boldsymbol{Y}_R(j\omega) \,=\, \boldsymbol{H}_R(j\omega)\,\boldsymbol{U}(j\omega) \tag{122}$$

---

[4] *Parseval's theorem* (for causal signals): if $\boldsymbol{x}(t) \in \mathcal{L}_2(\mathbb{R})$, then $\int_0^{+\infty} \boldsymbol{x}^T(t)\,\boldsymbol{x}(t)\,dt \,=\, \frac{1}{2\pi} \int_{-\infty}^{+\infty} \boldsymbol{X}^T(j\omega)\,\boldsymbol{X}(j\omega)\,d\omega$.

[5] In the following, the notation $\boldsymbol{M}^*$ is used to denote the complex–conjugate of the matrix $\boldsymbol{M}$

the quadratic cost function of the FS–LQR problem becomes:

$$
\begin{aligned}
J_{FS} \;&=\; \frac{1}{2\pi}\int_{-\infty}^{+\infty} \boldsymbol{X}^T(j\omega)\,\boldsymbol{Q}(j\omega)\,\boldsymbol{X}(j\omega) \;+\; \boldsymbol{U}^T(j\omega)\,\boldsymbol{R}(j\omega)\,\boldsymbol{U}(j\omega)\,d\omega \\[2mm]
&=\; \frac{1}{2\pi}\int_{-\infty}^{+\infty} \boldsymbol{X}^T(j\omega)\,\boldsymbol{H}_Q^*(j\omega)\,\boldsymbol{H}_Q(j\omega)\,\boldsymbol{X}(j\omega) \;+\; \boldsymbol{U}^T(j\omega)\,\boldsymbol{H}_R^*(j\omega)\,\boldsymbol{H}_R(j\omega)\,\boldsymbol{U}(j\omega)\,d\omega \\[2mm]
&=\; \frac{1}{2\pi}\int_{-\infty}^{+\infty} \boldsymbol{Y}_Q^*(j\omega)\,\boldsymbol{Y}_Q(j\omega) \;+\; \boldsymbol{Y}_R^*(j\omega)\,\boldsymbol{Y}_R(j\omega)\,d\omega \\[2mm]
&=\; \int_{0}^{+\infty} \boldsymbol{y}_Q^T(t)\,\boldsymbol{y}_Q(t) \;+\; \boldsymbol{y}_R^T(t)\,\boldsymbol{y}_R(t)\,dt
\end{aligned}
\tag{123}
$$

where the last identity has been obtained by applying the Parseval's theorem.

4) Introduce an "augmented–state" model that includes both the plant dynamics and the state–space models Σ_Q and Σ_R defined in (120) and (121):

$$
\Sigma_A: \quad \dot{\boldsymbol{x}}_A \;=\; \boldsymbol{A}_A\,\boldsymbol{x}_A \;+\; \boldsymbol{B}_A\,\boldsymbol{u}
\tag{124}
$$

with

$$
\boldsymbol{x}_A \triangleq \begin{bmatrix} \boldsymbol{x} \\ \boldsymbol{x}_Q \\ \boldsymbol{x}_R \end{bmatrix}, \qquad
\boldsymbol{A}_A \triangleq \begin{bmatrix} \boldsymbol{A} & \boldsymbol{0} & \boldsymbol{0} \\ \boldsymbol{B}_Q & \boldsymbol{A}_Q & \boldsymbol{0} \\ \boldsymbol{0} & \boldsymbol{0} & \boldsymbol{A}_R \end{bmatrix}, \qquad
\boldsymbol{B}_A \triangleq \begin{bmatrix} \boldsymbol{B} \\ \boldsymbol{0} \\ \boldsymbol{B}_R \end{bmatrix}
\tag{125}
$$

Regarding the dimensions, it holds that

$$
\boldsymbol{x}_A \in \mathbb{R}^{(n+n_Q+n_R)\times 1}, \quad
\boldsymbol{A}_A \in \mathbb{R}^{(n+n_Q+n_R)\times(n+n_Q+n_R)}, \quad
\boldsymbol{B}_A \in \mathbb{R}^{(n+n_Q+n_R)\times m}
\tag{126}
$$

5) With the augmented state $\boldsymbol{x}_A$ defined in (125), the cost function (123) can be rewritten (after some simple algebraic computations) as follows:

$$
J_{FS} \;=\; \int_{0}^{+\infty} \begin{bmatrix} \boldsymbol{x}_A^T & \boldsymbol{u}^T \end{bmatrix} \begin{bmatrix} \boldsymbol{Q}_A & \boldsymbol{N}_A \\ \boldsymbol{N}_A^T & \boldsymbol{R}_A \end{bmatrix} \begin{bmatrix} \boldsymbol{x}_A \\ \boldsymbol{u} \end{bmatrix} dt
\tag{127}
$$

with

$$
\boldsymbol{Q}_A \triangleq \begin{bmatrix} \boldsymbol{D}_Q^T\boldsymbol{D}_Q & \boldsymbol{D}_Q^T\boldsymbol{C}_Q & \boldsymbol{0} \\ \boldsymbol{C}_Q^T\boldsymbol{D}_Q & \boldsymbol{C}_Q^T\boldsymbol{C}_Q & \boldsymbol{0} \\ \boldsymbol{0} & \boldsymbol{0} & \boldsymbol{C}_R^T\boldsymbol{C}_R \end{bmatrix}, \qquad
\boldsymbol{N}_A \triangleq \begin{bmatrix} \boldsymbol{0} \\ \boldsymbol{0} \\ \boldsymbol{C}_R^T\boldsymbol{D}_R \end{bmatrix}, \qquad
\boldsymbol{R}_A \triangleq \boldsymbol{D}_R^T\boldsymbol{D}_R
\tag{128}
$$

6) The LQR problem for the augmented–state system Σ_A defined in (124) and the quadratic cost function (127)–(128) is a conventional LQR problem with "generalised" quadratic cost – see problem 2 of Sec. 7.1. The solution of such problem is reported in Thm. 2 of Sec. 7.1. In conclusion, note that the FS–LQR can be implemented as a standard LQR operating on the augmented state $\boldsymbol{x}_A$.

The frequency–dependent weights in (118) can be specified only for certain state or input vector components, while the remaining components are weighted with constant weights. To introduce frequency dependents weights only on certain state or input components, proceed as follows:

- suppose that only some weights in $\boldsymbol{Q}(j\omega)$ are frequency dependent. Without loss of generality, assume that the first $n' < n$ components of the state vector are weighted by a frequency dependent weight, i.e.

$$\boldsymbol{Q}(j\omega) = \operatorname{diag}\left\{\boldsymbol{Q}'(j\omega),\, \boldsymbol{Q}''\right\} \qquad \text{with} \qquad \boldsymbol{Q}'(j\omega) \in \mathbb{R}^{n'\times n'},\;\; \boldsymbol{Q}'' \in \mathbb{R}^{(n-n')\times(n-n')} \qquad (129)$$

Then

$$\boldsymbol{Q}(j\omega) = \boldsymbol{H}_Q^*(j\omega)\boldsymbol{H}_Q(j\omega) \qquad \text{with} \qquad \boldsymbol{H}_Q(j\omega) = \begin{bmatrix} \boldsymbol{H}'_Q(j\omega) & \boldsymbol{0} \\ \boldsymbol{0} & \boldsymbol{H}''_Q \end{bmatrix} \qquad (130)$$

Regarding the dimensions, it holds that

$$\boldsymbol{H}'_Q(j\omega) \in \mathbb{C}^{r'\times n'},\qquad \boldsymbol{H}''_Q \in \mathbb{R}^{r''\times(n-n')} \qquad (131)$$

where[6]

$$r' = \operatorname{rank} H'_Q = \operatorname{rank}\boldsymbol{Q}' \leq n' \qquad (132)$$

$$r' + r'' = r = \operatorname{rank}\boldsymbol{H}_Q = \operatorname{rank}\boldsymbol{Q} \leq n$$

Therefore, the state–space representation $\Sigma_Q = (\boldsymbol{A}_Q,\,\boldsymbol{B}_Q,\,\boldsymbol{C}_Q,\,\boldsymbol{D}_Q)$ for the transfer matrix $\boldsymbol{H}_Q(s)$ is such that

$$\boldsymbol{A}_Q = \boldsymbol{A}_{Q'},\qquad \boldsymbol{B}_Q = \begin{bmatrix} \boldsymbol{B}_{Q'} & \boldsymbol{0} \end{bmatrix},\qquad \boldsymbol{C}_Q = \begin{bmatrix} \boldsymbol{C}_{Q'} \\ \boldsymbol{0} \end{bmatrix},\qquad \boldsymbol{D}_Q = \begin{bmatrix} \boldsymbol{D}_{Q'} & \boldsymbol{0} \\ \boldsymbol{0} & \boldsymbol{H}''_Q \end{bmatrix} \qquad (133)$$

where $\Sigma_{Q'} = (\boldsymbol{A}_{Q'},\,\boldsymbol{B}_{Q'},\,\boldsymbol{C}_{Q'},\,\boldsymbol{D}_{Q'})$ is a state–space realisation of the transfer matrix $\boldsymbol{H}'_Q(s)$.

- suppose that only some weights in $\boldsymbol{R}(j\omega)$ are frequency dependent. Without loss of generality, assume that the first $m' < m$ components of the input vector are weighted by a frequency dependent weight, i.e.

$$\boldsymbol{R}(j\omega) = \operatorname{diag}\left\{\boldsymbol{R}'(j\omega),\, \boldsymbol{R}''\right\} \qquad \text{with} \qquad \boldsymbol{R}'(j\omega) \in \mathbb{R}^{m'\times m'},\;\; \boldsymbol{R}'' \in \mathbb{R}^{(m-m')\times(m-m')} \qquad (134)$$

Then

$$\boldsymbol{R}(j\omega) = \boldsymbol{H}_R^*(j\omega)\boldsymbol{H}_R(j\omega) \qquad \text{with} \qquad \boldsymbol{H}_R(j\omega) = \begin{bmatrix} \boldsymbol{H}'_R(j\omega) & \boldsymbol{0} \\ \boldsymbol{0} & \boldsymbol{H}''_R \end{bmatrix} \qquad (135)$$

Therefore, the state–space representation $\Sigma_R = (\boldsymbol{A}_R,\,\boldsymbol{B}_R,\,\boldsymbol{C}_R,\,\boldsymbol{D}_R)$ for the transfer matrix $\boldsymbol{H}_R(s)$ is such that

$$\boldsymbol{A}_R = \boldsymbol{A}_{R'},\qquad \boldsymbol{B}_R = \begin{bmatrix} \boldsymbol{B}_{R'} & \boldsymbol{0} \end{bmatrix},\qquad \boldsymbol{C}_R = \begin{bmatrix} \boldsymbol{C}_{R'} \\ \boldsymbol{0} \end{bmatrix},\qquad \boldsymbol{D}_R = \begin{bmatrix} \boldsymbol{D}_{R'} & \boldsymbol{0} \\ \boldsymbol{0} & \boldsymbol{H}''_R \end{bmatrix} \qquad (136)$$

where $\Sigma_{R'} = (\boldsymbol{A}_{R'},\,\boldsymbol{B}_{R'},\,\boldsymbol{C}_{R'},\,\boldsymbol{D}_{R'})$ is a state–space realisation of the transfer matrix $\boldsymbol{H}'_R(s)$.

Note: for the existence of a solution of the "auxiliary LQR problem" for the augmented–state model Σ_A, it is necessary that $\boldsymbol{D}_R$ is a nonsingular matrix, so that $\boldsymbol{R}_A$ is positive definite. Hence, the elements of the transfer matrix $\boldsymbol{H}'_R(s)$ must be proper transfer functions, but not *strictly* proper, otherwise $\boldsymbol{D}'_R$ and $\boldsymbol{D}_R$ are not full–rank matrices, and $\boldsymbol{R}_A$ is not positive definite.

---

[6]Remind that both $\boldsymbol{Q}'(j\omega)$ and $\boldsymbol{Q}''$ are positive *semidefinite*, so that $\operatorname{rank}\boldsymbol{Q}'(j\omega) \leq n'$ and $\operatorname{rank}\boldsymbol{Q}'' \leq n - n'$.